Air Force Institute of Technology

AFIT Scholar

Theses and Dissertations

Student Graduate Works

3-14-2014

Applying KAM Theory to Highly Eccentric Orbits

Adam B. Dunk

Follow this and additional works at: https://scholar.afit.edu/etd

APPLYING KAM THEORY TO HIGHLY ECCENTRIC ORBITS

THESIS

Adam B. Dunk, Captain, USAF

AFIT-ENY-14-M-19

DEPARTMENT OF THE AIR FORCE
AIR UNIVERSITY

AIR FORCE INSTITUTE OF TECHNOLOGY

Wright-Patterson Air Force Base, Ohio

AFIT-ENY-14-M-19

APPLYING KAM THEORY TO HIGHLY ECCENTRIC ORBITS

THESIS

Presented to the Faculty

Department of Aeronautics and Astronautics

Graduate School of Engineering and Management

Air Force Institute of Technology

Air University

Air Education and Training Command

in Partial Fulfillment of the Requirements for the

Degree of Master of Science in Astronautical Engineering

Adam B. Dunk, B.S.A.E.

Captain, USAF

March 2014

AFIT-ENY-14-M-19

APPLYING KAM THEORY TO HIGHLY ECCENTRIC ORBITS

Adam B. Dunk, B.S.A.E.
Captain, USAF

Approved:

//signed//	26 Feb 2014
William E. Wiesel Jr., PhD (Chairman)	Date

//signed//	26 Feb 2014
Eric D. Swenson, PhD (Member)	Date

//signed//	26 Feb 2014
LtCol Ronald J. Simmons, PhD (Member)	Date

AFIT-ENY-14-M-19

Abstract

THIS research applies KAM theory to highly eccentric orbits for earth orbiting satellites by using spectral methods to find the three basis frequencies resulting from earth's geopotential. Once a torus is created from these frequencies, its dynamics data can be compared to the position data of an integrated data set over multiple orbit types, specifically, orbits with varying eccentricity. The analysis shows that many eccentric orbits are actually KAM tori when the only perturbation is the earth's geopotential. The residuals agree to 10s of meters in most cases. This research also outlines many of the limitations of the current method and gives recommendations for further study and real-world applications. Applications focus on space debris and non-operational satellites.

Acknowledgements

I'd like to thank my amazing wife for being supportive throughout this long process. Thank you for your selflessness. You have been a wonderful encouragement and source of joy during the course of my studies. I'd also like to recognize my research advisor, Dr. Wiesel. Thank you for your guidance and shepherding and for your dedication to helping me see this project through to completion. It has been a joy to work with you.

Adam B. Dunk

Table of Contents

List of Figures

List of Tables

List of Symbols

Symbol   Definition

ϵ small perturbation parameter

$\mathcal{H}$ Hamiltonian

Subscripts

integrable   Referring to an integrable function

perturbation   Referring to a perturbation function

List of Acronyms

Acronym	Definition
DFT	Discrete Fourier Transform
DORIS	Doppler Orbitography and Radiopositioning Integrated by Satellite
ECEF	Earth Centered Earth Fixed
EGM-96	Earth Gravitational Model 1996
ERS-1	European Remote-Sensing Satellite
FFT	Fast Fourier Transform
GSFC	Goddard Space Flight Center
GPS	Global Positioning System
GRACE	Gravity Recovery and Climate Experiment
HEO	Highly Elliptical Orbit
KAM	Kolmogorov-Arnold-Moser
LEO	Low Earth Orbit
NASA	National Aeronautics and Space Administration
OSU-91A	Ohio State University 1991-A
RR	Range Rate
S2	Satellite to Satellite Tracking
TOPEX	Topography Experiment

APPLYING KAM THEORY TO HIGHLY ECCENTRIC ORBITS

I. Introduction

1.1   Motivation

In 2009, the Iridium 33 and Kosmos 2251 satellite collided in outer space. This was the first unintentional collision at high speeds between two artificial satellites in the earth's orbit [1]. Iridium 33 was an operational satellite, and Kosmos was out of service for 13 years. Besides completely disabling Iridium 33, the collision created thousands of pieces of debris, posing a threat to other satellites in the vicinity and remaining in orbit for several years. Preventing events like this one is the motivation for this research. Are there ways to increase the accuracy of earth-satellite dynamics predictions? Can we know where a satellite will be over long periods of time with greater certainty than current methods?

1.2   Approach

The engine for this research are the results generated from spectral analysis methods and KAM tori theory. The idea is that the earth's geopotential causes a satellite/orbit to rotate at three frequencies: anomalistic, precession, apsidal. The earth's geopotential is known, therefore, these three frequencies can also be found. Once known, KAM theorem states that the motion and dynamics for those three frequencies will lie on a 6-dimensional torus. The method to derive this torus results from integrating orbital data based on the earth's geopotential, using spectral methods to find the basis frequencies, creating a torus from those frequencies, and then computing the residuals between the torus position data and the integrated data. The size of the residuals will determine the accuracy of this

1

particular approach. This methodology has been successfully demonstrated by Wiesel for small, circular orbits [21].

1.3 Problem Statement

This research aims to push the limits of this methodology and examine if it is viable for highly eccentric orbits. The research questions include:

- Can KAM theory be used to model dynamics for earth satellites in highly eccentric orbits?

- Will this method capture a more accurate picture of the true dynamics?

- How accurate are the results?

This research will also highlight many of the limitations of the proposed methodology, identify areas for future study, and give recommendations for real-world usage

1.4 Results

The results of this research are extremely promising. Though there are some limitations, such as, air drag, resonance, and commensurate frequencies, the results show that eccentric orbits do resemble KAM tori. Residuals are at the level of tens of meters between 0.05 and 0.5 eccentricity over four years. A few improvements in the software and coding could potentially have the residuals for even higher eccentricities at the same of accuracy. Potential real-world uses include improving prediction accuracy for space debris and "fly and forget" satellites.

II. Background

2.1 A Brief History of Celestial and Orbital Mechanics

Johannes Kepler, in 1609, compiled a 650+ page book that dramatically changed the way humans would understand the movement of the heavenly bodies [2]. Though unwittingly committing a couple blunders, Kepler published *Astronomia Nova ΑΙΤΙΟΛΟΓΣΤΟΣ seu physica coelestis, tradita commentariis de motibus stellae Martis ex observationibus G.V. Tychonis Brahe*, in which he details the arduous process of examining the orbit of Mars. Fortuitously for Kepler, his math mistakes essentially "canceled," and he was able to arrive at the following principles from his observations:

1. Planetary orbits are elliptical in shape with the sun at one focus.
2. "The velocity of a planet varies in such a way that a line joining the planet to the sun sweeps out equal areas in equal times [2]."

Ten years later, Kepler would add a third discovery to this list, now known as "Kepler's Third Law:"

3. The square of the orbital period of a planet is proportional to the cube of the semi-major axis of its orbit.

In 1687, Isaac Newton would prove Kepler's discoveries after publishing another one of the most important works in scientific history, *Philosophiae Naturalis Principia Mathematica*, or now known simply as *Principia*. In it, he established the foundation of classical mechanics, laws of motion, and the universal law of gravitation. The *Principia* also *derives* Kepler's laws of planetary motion (which Kepler found *empirically*). The combination of Kepler and Newton's work allowed astronomers to understand planetary motion in a perfect or ideal scenario, and resulted in what today is called the "2-body problem."

A quest for more accurate dynamics of the solar system (solving the *n*-body problem) gave way for more exhaustive research efforts of Newton, Euler, Lagrange, Jacobi, Poincar*é*, and many others. The King of Sweden, Oscar II, even famously offered a prize for any mathematician who could solve the 3-body problem. Ultimately, the prize was awarded to Poincar*é* (though he did *not* solve the problem) for his efforts leading to the theory of chaos. However, in 1906, Karl Sundman did analytically prove the convergence of an infinite series as a solution to the problem, but the slow rate of convergence makes it impractical for dynamics applications.

In the absence of an analytical solution to the workings of the universe, scientists are left with perturbation theory as the current method for approximating celestial and satellite dynamics. Perturbation theory attempts to approximate a solution to an unsolvable problem, i.e., the *n*-body problem, by starting with a known solution to a closely related problem, i.e., the 2-body problem, and adding a series expansion of small changes to the dynamics. The assumption here is, of course, that small changes in the dynamics will result in small changes in the approximated solution.

Borrowing from the work of Lagrange and later Hamilton, perturbation theory for dynamical systems can be written as a known integrable Hamiltonian function plus the perturbation. It is easily visualized in Equation (2.1), where ϵ is a small perturbation parameter.

$$\mathcal{H} = \mathcal{H}_{integrable} + \epsilon\mathcal{H}_{perturbation} \tag{2.1}$$

Solving this equation with regards to celestial bodies, orbital mechanics has been the focus for many researches within these fields for hundreds of years. The ordered terms in the series expansion solution to this equation are well known, but they are limited for use over short time periods. This is because the difference between eigenvalues located in the denominators of each order become exceedingly small, which, if occurring in higher order

terms can elevate their significance above even the first order term. This issue, known as the small-divisor problem, can cause solutions to diverge over large timescales, and it had stymied further advancements in the field for a period of time.

Yet, it is no small matter that the efforts of many heroes in the dynamics research field had successfully matured perturbation theory to provide *approximate* solutions over *short* time periods, with solutions diverging greatly as time goes on.

2.2 KAM Theory Overview

In 1954, A.N. Kolmogorov brought his hefty discoveries to the table of dynamics research. While limited in application to dynamical systems that are nondegenerate, integrable (or nearly integrable), with *sufficiently small* perturbations and free of resonances, Kolmogorov was able both overcome the small divisor problem and posit that the resulting dynamics would lie on the surface of an invariant torus. His exact theorem states:

> **Theorem.** *If an unperturbed system is nondegenerate, then for sufficiently small conservative Hamiltonian perturbations, most non-resonant invariant tori do not vanish, but are only slightly deformed, so that in the phase space of the perturbed system, too, there are invariant tori densely filled with phase space curves winding around them conditionally periodically, with a number of independent frequencies equal to the number of degrees of freedom. These invariant tori form a majority in the sense that the measure of the complement of their union is small when the perturbation is small.* [3]

These conditions may seem restrictive for applicable, real-world research, but Wiesel has demonstrated that some earth satellite orbits resemble KAM tori [21–24]. This research aims to better understand the boundaries of these assumptions by venturing into orbits that are highly eccentric.

2.2.1 Integral Dynamical Systems.

This research will consider dynamical systems that can be described by a Hamiltonian, that is, a single, comprehensive function that represents the dynamics of that system. Two properties of a Hamiltonian dynamical system are:

1. The preservation of its symplectic nature,

2. The preservation of its volume. [5]

The first property reflects that the fact that the manifold in phase space remains invariant or is nondegenerate. Applying Liouville's theorem to the second property shows that invariant tori remain constant in phase space volume after perturbations, even though they become deformed [5].

Specifically, for conservative, time-independent, dynamical systems (like earth orbiting satellites), an examination of the Poisson bracket for the Hamiltonian system will quickly yield an integral of the motion, as the Hamiltonian does not change over time. In fact, there are $2N$ integrals of the motion in a system with N degrees of freedom. Several methods can be used to find these integrals, including Poisson bracket properties, Jacobi's identity, and Hamilton-Jacobi theory [17, 20]. A system is considered to be an *integrable* system if N integrals of the motion are identified, and it is exactly *solvable* if all the integrals of the motion are found.

The dynamics of earth orbiting satellites are not only conservative and time-independent but are also *periodic*. The motion of this type of system (Hamiltonian, integrable, periodic) is specifically known as quasi-periodic or multiply periodic motion. Simply stated, multiply periodic motion is periodic motion with an N number of fundamental frequencies, and this motion can be easily modeled with a Fourier series or action-angle variables. Equation (2.2) shows the Hamiltonian converted to the action-angle variable form

$$\mathcal{H}(\mathbf{I}, \theta) = \mathcal{H}_0(\mathbf{I}) + \epsilon\mathcal{H}_1(\mathbf{I}, \theta), \tag{2.2}$$

where

$$\dot{I}_j = 0 \tag{2.3}$$

and

$$\dot{\theta}_j = \frac{\partial\mathcal{H}(I)}{\partial I_j} = \omega_j(I). \tag{2.4}$$

Kolmogorov derived his theorem (stated in §2.2) from Equation (2.2). His research outlined a proof (later proved by Arnold and Moser) that showed the motion of a body in such a dynamical system will lie on the surface of a torus in phase space. It was also shown that the torus will have dimensions equivalent to the number of degrees of freedom of the system. (In the case of earth orbiting satellite, motion lies on the surface of a 3-dimensional torus in *6-dimensional space*, as there are six degrees of freedom: three in the position and three in the velocity). Kolmogorov arrived at this discovery by:

1. Assuming an N-dimensional torus (or tori) exists,

2. Transforming coordinates so that the perturbed Hamiltonian is only a function of the new action-angle coordinates,

$$\mathcal{H}(\mathbf{I}, \theta) = \mathcal{H}'(\mathbf{I}'), \tag{2.5}$$

3. Solving the Hamilton-Jacobi equation for the following generating function (Equation (2.6) using a Newton-Rhapson algorithm in order to bypass the small divisor problem:

$$\mathcal{H}'(\mathbf{I}') = \mathcal{H}\left(\frac{\partial S(I', \theta)}{\partial\theta}, \theta\right) \tag{2.6}$$

Proving the existence of tori and describing motion for object in an integrable, periodic, Hamiltonian dynamics system was a brilliant breakthrough in the timeline of dynamics history. However, there are limitations that constrain its use in real-world applications.

2.2.2 KAM Theory Limitations.

In order to converge on a particular solution, Kolmogorov notes that perturbations must be "sufficiently small" and the fundamental frequencies must be "sufficiently incommensurate [3]." When these conditions are met, the system is perpetually stable.

A "sufficiently small" perturbation can often be ill defined and is typically dependent on the dynamical system being studied. When addressing the "sufficiently small" perturbations issue in the context of celestial mechanics, Celletti remarks when ϵ (the perturbation parameter) is too large, applying KAM theory to solar system dynamics "leads to very poor 'practical' results." He continues to to explain that this parameter is typically determined by the size of mass ratios, which for the solar system dynamics can be relatively big when compared to earth-satellite dynamics [7]. Ratios of satellite mass compared to the earth are minuscule. In fact, Wiesel, Bordner, and Craft has all demonstrated overcoming any issues with this limitation when applied to satellite applications [5, 8, 21]. It is, therefore, very unlikely that this limitation would ever be transgressed for this type of research.

However, having "commensurate" or "nearly commensurate" frequencies can be a problem with specific types of orbits. As suggested by the name itself, commensurate frequencies will resonate, resulting in chaotic or unbounded motion. This can lead to convergence problems when integrating as well as frequency identification issues when using numerical spectral methods in trying to "back-out" KAM tori structures. Bordner ran into this problem when analyzing GPS orbits, stating, "Individual spectral lines cannot be identified when basis frequencies are nearly commensurate when using *practical* timespans

[5]." It is possible to stumble into the same problem if analyzing orbits at or near the critical inclination (or any known resonance), in which case a fundamental frequency would drop out all together. Poincar$\acute{e}'s$ method of sections can help identify both chaotic and stable regions and better inform the researcher as to which regions may be fertile ground for KAM tori [9].

2.2.3 Additional Information.

This research will capitalize on the results and applications that are a benefit of the theorem. If the reader desires to see the detailed derivations and proofs that are a part of KAM theory, these English translations [3, 13, 18] would fully satisfy any longing for a more comprehensive walkthrough.

2.3 KAM Theory Application to Earth Satellites

Over its 60 year history, KAM theory has been applied to the N-body problem, celestial mechanics, biological dynamics, and it has been studied among mathematicians and theorists [3, 6, 10, 11]. However, until the research conducted by Wiesel in 2007, no one has ventured to apply KAM theory to earth orbiting satellites. Wiesel and his army of student researchers have done much to advance KAM theory applications to this area. The premise of these research efforts stems from three distinct fundamental frequencies observed in satellite motion due to the earth's geopotential. These frequencies and effects of the earth's geopotential are already well known:

- The anomalistic frequency, ω_1, is nearly the mean motion of the satellite in its orbit, more commonly known as the Keplerian frequency. Moreover, this is the resulting mean motion after taking into account secular effects from the earth's geopotential. See Equation (2.7).

- The precession frequency, ω_2, is a combination of the earth's rotation rate and the rate of nodal regression. (Note: The earth's rotation rate is added here because

9

this research uses the Earth Centered Earth Fixed (ECEF) reference frame.) See Equation (2.8).

- The apsidal regression rate, ω_3, is the rotation rate of the orbit about its normal vector. It can also be thought of as the movement of the argument of perigee. See Equation (2.9).

Wiesel was the first to explore the possibility that these frequencies could be the basis frequencies of a torus [21]. He was able to confirm the that KAM tori do exist and that many of earth's satellites lie on them. His methods included numerically integrating an orbital trajectory (using National Aeronautics and Space Administration (NASA)'s Earth Gravitational Model 1996 (EGM-96) gravity model, degree and order 20) and then applying Laskar frequency algorithms to pick off the fundamental frequencies. After identifying these frequencies, Wiesel fit them to a Fourier series and compared it to a least squares fit of the integrated orbit. His results showed accuracy at the resolution of tens of meters after 20 days, thereby validating this approach to earth satellite dynamics. This research attempts a similar approach looking specifically at highly eccentric orbits. Wiesel's method separates itself from perturbation theory in that the definite frequencies for satellite motion about earth can be explicitly found, and any resulting errors between predictions and the actual data is directly attributable to outside perturbations. In other words, the torus is the exact (or known) solution, and perturbation theory can use that solution as the starting point for approximations to determine perturbations other than the earth's geopotential. Wiesel also conveniently demonstrated an analytical method to approximate these three frequencies (on the order of J2):

$$\omega_1 \approx \sqrt{\frac{\mu}{\alpha^3}} \left\{ 1 - \frac{3 J_2 R_\oplus^2}{2 \alpha^2 (1 - e^2)^3 / 2} \left(\frac{3}{2} \sin^2 i - 1 \right) \right\} \tag{2.7}$$

$$\omega_2 \approx \omega_\oplus + \frac{3 \sqrt{\mu} J_2 R_\oplus^2}{2 \alpha^7 / 2 (1 - e^2)^2} \cos i \tag{2.8}$$

$$\omega_3 \approx -\frac{3\sqrt{\mu}J_2R_\oplus^2}{2\alpha^7/2(1-e^2)^2}\left(\frac{5}{2}\sin^2 i - 2\right) \tag{2.9}$$

There are several relationships that exist between these frequencies and the orbital elements which are worth noting. As intuition would dictate, the anomalistic frequency *decreases* as orbital altitude, or semi-major axis, *increases* as the term is dominated by the Keplerian mean motion. Secondly, as inclination approaches 90°, the precession frequency simply becomes the earth's rotation rate, since the nodal regression rate from the geopotential drops out due to the cosine term. Finally, and perhaps most importantly for this research, the apsidal regression rate approaches zero when the orbit approaches the critical inclination, 63.4°. Figure 2.1 shows this revelation visually, as this is not easily discovered from examining the equation itself. Craft concludes in his research that the accuracy of KAM tori may decrease as the apsidal frequency approaches zero [8]. He says, "As ω_3 falls closer and closer to a zero value, the trajectory knowledge must be more and more accurate over a longer and longer time to accurately determine the basis frequencies,...,In the limit where $i = i^* = 63.4\ deg$, the basis frequency set $\overline{\omega} = [\omega_1,\omega_2,\omega_3]$ would be said to be *commensurable* (i.e., two or more elements of the set have a common divisor), violating the Diophantine condition[1],...,and leading to an exacerbated problem of small divisors. In this case, the torus would be practically incalculable." He continues to explain, however, that for cases where $i\text{-}i^* \approx 0$, the torus may actually be able to be expressed with two fundamental frequencies. Craft also notes that the "transition region" for less than desirable accuracy results occurs when 0.0017 rad/s $> \omega_3 > 0$. This rate will vary with eccentricity, but for

---

[1]

$$\left|\sum_{i=1}^{N}\alpha_i\omega_i\right| \geq C\,\|\alpha\|^{-\nu}\,for\ all\ \alpha = \{\alpha_1, \alpha_2, ..., \alpha_n\} \in Z^n$$

where $C \geq 0$ and $\nu \geq 0$.

highly eccentric orbits (on the order of $e = 0.75$), this is about 63.4 ± 0.0349 degrees. In light of this, this research will *not* be examining orbits in this region. This is, perhaps, an area of future research.
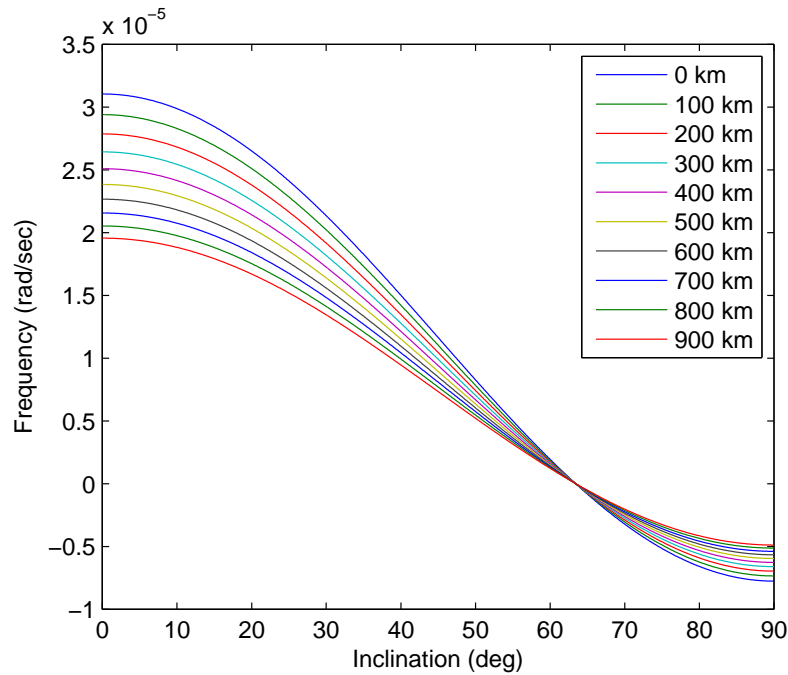
Figure 2.1: Apsidal frequency of an eccentric orbit over all inclinations in LEO.

Since 2007, Wiesel has advanced his methods by demonstrating two methods for constructing tori. The first algorithm numerically fits a KAM torus to numerically integrated orbit data, and the second algorithm extracts the Fourier coefficients from a numerically integrated Fourier transform [22]. In a later paper, Wiesel also published how to linearize solutions from a reference KAM torus [23].

Bordner uses slight variations on these methods in his research [5]. He conducted frequency analysis on *actual* orbit data from GPS satellites to construct KAM tori. During the frequency analysis, he quickly discovered that the GPS satellites had two frequencies that were commensurate, because the GPS constellation lies *exactly* on the earth's 2:1

resonance. An issue concerning the apsidal frequency also crept up in the analysis. Due to the small sample size of data and the long period of the apsidal frequency, Bordner was not able to meet the minimum sampling rate required to satisfy the Nyquist-Shannon Theorem criteria. These issues inevitably led Bordner's tori prediction fits to be on the order of tens of kilometers over a ten week period, a stark discontinuity from Wiesel's ten *meter* accuracy [21]. Finally, without the ability to compare to Wiesel's results (as the fundamental limitations of the theorem were breached), the effects of third-body perturbations remain unclear.

Little's research also attempted to fit KAM tori to real satellite ephemeris data [16]. He modeled the data of two NASA satellites, Jason and Gravity Recovery and Climate Experiment (GRACE), with some success. However, with air drag being a major dynamics contributor for LEO satellites (which is not accounted for in this application of KAM theory), Little's results demonstrated one kilometer accuracy over a two week period.

Craft, in his research, wanted to take advantage of the potential long term accuracy given by KAM theory and apply it to satellite formation flights. Over a 60 day window, these satellite clusters showed drift rates in the range of *nanometers* when having a 10-100 meter separation. However, the accuracy is proportional to the amount of separation, perhaps limiting its use[8].

2.4   Summary

KAM theory was a brilliant realization in 1954, and, remarkably, is it still being integrated into the mindsets of modern dynamicists. Its principles happen to fit neatly into the study of earth satellite dynamics, making long term, accurate dynamics predictions a real possibility. The research conducted by Wiesel, Bordner, Craft, and Little has shown that 1) it is possible to have very accurate predictions over long periods of time making it comparable (and in many cases *better*) than current methods, and 2) this theory can be extended to many different types of satellite applications, from LEO satellites, GPS

accuracy, and even formation flying. This research hopes to fill in more of the unknowns in regards to the applicability of KAM theory to other orbit types, specifically, Highly Elliptical Orbit(s) (HEO)s. If a Highly Elliptical Orbit (HEO) is found to lie on a torus, the Air Force could use this information to improve tracking and prediction of "dead" objects in the space catalog.[2] Ultimately, this could lead to less maneuvering (which translates into fuel savings and increased lifespan) for "live" satellites. And for "dead" satellites, accurate position data can be known for years in advance, allowing much improved collision prediction capabilities. However, the results from this research are limited in the sense that only forces from the earth's geopotential are taken into account. Further research would be needed to account for addition forces, such as air drag and third body effects. Wiesel has shown that it is possible to use perturbation theory with the KAM torus as the known solution (rather than the Two Body Problem) and find the approximate solutions by using similar dynamics techniques [24].

---

[2]Bordner and Little have shown that large, continuous datasets would be needed. "Live" satellites are subject to stationkeeping maneuvers, essentially creating a new dataset for each maneuver.

III. Method

The approach to meeting the core objectives of this research can be summarized in the following manner: create orbital data, analyze the data to find KAM tori frequencies, create KAM tori position and velocity data from those frequencies, and, finally, compare the KAM tori data with the original integration to determine accuracy. Essentially, this research is calculating residuals and conducting analysis between a model (KAM theory) and simulated data.

3.1   Creating Orbital Data for Analysis

There are two means of acquiring orbital data: create data or use actual data. Wiesel and Craft used an integrator to propagate a set of equations of motion over time, thereby creating position and velocity vectors at each time step. Border and Little used actual orbital data in their research. The advantages of one over the other are distinct. Creating an integrated data set means that the data is only as good as the integrator itself. If there are any perturbations forces that are not included in the integration, then they will not be included in the data. Likewise, if there are errors (or rounding, or truncating of perturbations) in the dynamics integrator, those errors will also be a part of the data. Overtime, these errors can become quite large. However, a good integrator will allow its data to be matched with the KAM torus model's data, while keeping errors small. This is quite advantageous for the current research.

The technique of using actual data can also pose difficulties. Most notably, acquiring the actual data it not currently possible due to security concerns. Only a limited amount of published ephemeris data exists and it may not come in the desired format, that is to say, the time period, time steps, units, etc. may be incompatible, altered, or missing altogether. This type of data set may also be riddled with maneuvers or gaps in data captures, presenting

additional challenges. Maneuvers must be resolved to compare dynamics, and every maneuver essentially starts a "new" dataset, which can greatly shorten what was a long data set. Data gaps, on the other hand, usually must be "filled in" to be compatible with software analysis. Another consideration when using actual data is that *all* perturbations are acting on that requested object. This may or may not be advantageous depending on the type of research. Finally, using actual data can have implications on the availability of desired orbits. Retrieving all of the exact research orbits for a specific duration with no orbital maneuvers will prove to be a very difficult if not impossible task.

This research is specifically looking at the orbital frequencies caused by the earth's geopotential, and it requires a comprehensive examination of a large subset of orbit types. That makes creating integrated data sets the clear choice for this research.

3.1.1 *Equations of Motion and the Hamiltonian.*

In the ECEF frame, creating the Hamiltonian to describe satellite motion starts by defining the specific momenta, p_n [21].

$$p_x = \dot{x} - \omega_\oplus y \tag{3.1}$$

$$p_y = \dot{y} + \omega_\oplus y \tag{3.2}$$

$$p_z = \dot{z} \tag{3.3}$$

In these equations, x, y, and z describe the satellite position and $\omega_\oplus$ is the rotation rate of the earth. Constructing the Hamiltonian is further defined as

$$H = \sum_i p_i \dot{q}_i - L, \tag{3.4}$$

where L is the difference between the kinetic (T) and potential (V) energy,

$$L = T - V. \tag{3.5}$$

Substituting in the kinetic and potential energies into Equation (3.4) yields the Hamiltonian in its final form [20]:

$$
\begin{aligned}
H = \frac{1}{2}(p_x^2 + p_y^2 + p_z^2) + \omega_\oplus \times (yp_x - xp_y) \\
- \frac{\mu}{r} \sum_{n=0}^{\infty} \sum_{m=0}^{n} \left(\frac{r}{R_\oplus} \right)^{-n} P_n^m (\sin \delta) \\
\times [C_{nm} \cos(m\lambda) + S_{nm} \sin(m\lambda)].
\end{aligned}
\tag{3.6}
$$

The specific terms in Equation (3.6) are as follows:

μ: Gravitational parameter

r: Radius of the satellite from the center of the earth, $r = \sqrt{x^2 + y^2 + z^2}$

$R_\oplus$: Radius of the earth

P_n^m: Legendre polynomials

C_{nm}: and S_{nm} Gravity field coefficients

δ: Geocentric latitude, $\sin \delta = \frac{z}{\sqrt{x^2+y^2}}$

λ: East longitude, $\tan \lambda = \frac{y}{x}$

The numerical integration technique of choice for propagating these equations of motion is the Hamming integrator. Because the Hamming integrator is not symplectic, meaning that it does not conserve the Hamiltonian, we can check its accuracy for each time step [8]. This is computed by subtracting and examining the Hamiltonian values to make certain that δH is small for all time. It should be noted, that the integration is symmetrically split over the desired time interval, centered at zero, to meet spectral analysis requirements. Therefore, the final data set is the combination of both a backwards and forwards integration. Coincidentally, this time interval technique, [-T,T], reduces the total Hamiltonian error, as compared to a [0,2T] time interval integration. If the Hamiltonian

error becomes any higher than 10^{-12}, meter level skews in accuracy can occur in the residuals. The number of time steps and integrations steps have been chosen such that this threshold is not violated.

3.1.2 Earth's Geopotential.

Modeling the earth's geopotential correctly within the integrator/propagator is critical, since the dynamics result from it directly. Equation (3.7) is a combination of the zonal, sectoral, and tesseral harmonics of the earth's geopotential, and this research will include all effects up to $m = 20$ and $n = 20$.

$$V = -\frac{\mu}{r} \sum_{n=0}^{\infty} \sum_{m=0}^{n} \left(\frac{r}{R_\oplus}\right)^{-n} P_n^m (\sin \delta) \times [C_{nm} \cos(m\lambda) + S_{nm} \sin(m\lambda)] \qquad (3.7)$$

As a reminder, zonal harmonics describe the earth's mass allocation in bands of latitude, and these terms are isolated when $m = 0$ in Equation (3.7). The most commonly known and strongest perturbation due to zonal harmonics is J_2. This is a result of the bulging band of latitude around the earth center, which reflects the oblateness of the earth. While not extremely large when compared to the Newtonian potential term, only about one thousandth of the size, it does have a significant effect on orbits over time. Similarly, sectoral harmonics account for mass distributions in bands of longitude. These terms appear mathematically when $m = n$. Finally, tesseral harmonics describe the mass of areas or regions of the earth where it is not quite a perfect sphere, and these terms appear when $m \neq n \neq 0$. Figure 3.1, Figure 3.2, and Figure 3.3 show a visual depiction of each type of harmonic. In each figure, the shaded areas represent extra mass, and the numbering, i.e., "2,0," represents n and m respectively. For a thorough analysis of the geopotential and its derivations, c.f. [19].

EGM-96 is an earth gravity model that is complete through degree and order 360. It was formed by combining data from Ohio State University 1991-A (OSU-91A), Goddard
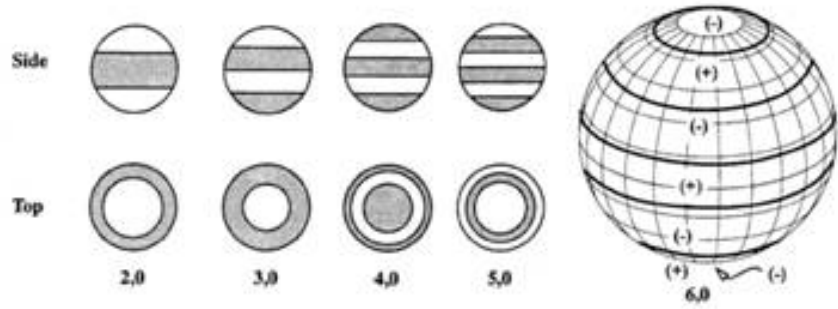
Figure 3.1: Zonal Harmonics of the Earth's Geopotential (ref. [19])
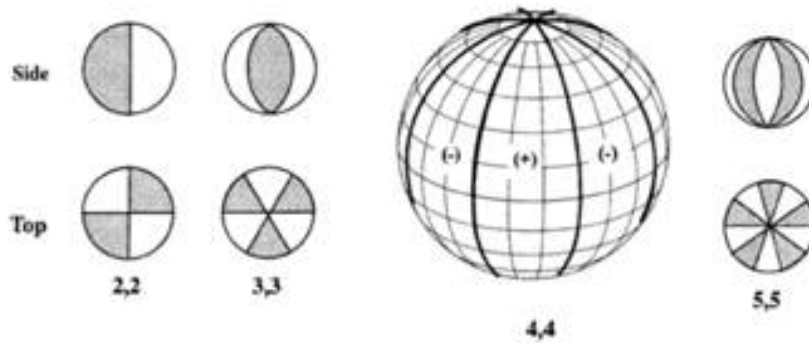
Figure 3.2: Sectoral Harmonics of the Earth's Geopotential (ref. [19])

Space Flight Center (GSFC), University of Texas at Austin, European communities, and Defense Mapping Agency [19]. The gravitational data for this model was collected with over 30 different satellites, including European Remote-Sensing Satellite (ERS-1), Geosat,
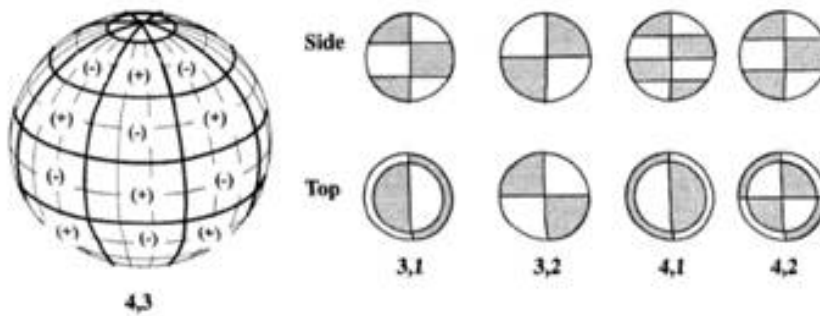
Figure 3.3: Tesseral Harmonics of the Earth's Geopotential (ref. [19])

19

and Topography Experiment (TOPEX) using all data types (optical, laser, Doppler, Range Rate (RR), Satellite to Satellite Tracking (S2), Global Positioning System (GPS), and Doppler Orbitography and Radiopositioning Integrated by Satellite (DORIS))[19]. The combined result is an extremely accurate earth gravity model suitable for orbits between 1-144 degrees inclination and 600-2,000, 5,900, and 35,000 km perigee height [19]:

Intensive computing requirements warrant the need to truncate EGM-96 to $n,m = 20$ for faster simulations in the preliminary research stage. It would be possible to use a higher order geopotential, e.g., 50x50 or even 360x360, should this initial research succeed and there is an additional need to have even better fidelity in the results.

3.1.3   Orbit Selection and Considerations.

Several considerations were taken into account when choosing orbits to analyze.

1. Have a control orbit to duplicate the results of previous research.

2. Complete the objective of analyzing eccentric orbits.

3. Choose orbits away from resonance caused by the earth's geopotential.

4. Choose eccentric orbits that will have incommensurate frequencies.

5. Choose an integration time period large enough such that the Nyquist-Shannon Theorem criteria for the smallest orbital basis frequency is met.

Having a control orbit is important for two reasons. First, it validates the mathematical approach and implementation of the theory if the results match with previous research. In other words, it demonstrates that the starting point for this research is correct and eliminates any question of the soundness of the mathematical approach as a concern for error. Secondly, and similarly, it validates the functionality of the software packages being used in this research.

Completing the objectives for analyzing eccentric orbits seems fairly obvious, however, some questions remain as to how this should look. A good study of "highly" eccentric orbits should include orbits that meet the eccentricity many satellites are currently

20

using. However, a slightly better approach is to examine if KAM tori theory remains viable as eccentricity scales upwards. This would allow one to see how high eccentricity can be elevated before the theory begins to breaks down, if at all. Therefore, it would be useful to study a wide range of eccentricities, perhaps varying them over a specific orbit prototype.

Choosing orbits aways from the earth's resonance is fairly straightforward. The resonance effect experienced in orbits is directly proportional to the orbit's semi-major axis. Avoiding the semi-major axis values in Table 3.1.3 will avoid most areas of resonance. However, as noted before, other types of resonance do exist. Molniya, polar, and sun-synchronous orbits will not be considered.

A nearly integrable, perturbed, periodic system will have variant tori or commensurate frequencies only a small percentage of the time [4]. Invariant, deformed tori mostly survive. It is when orbits are located around resonance or when one or more of the basis frequencies approaches zero that they do not. These areas are known (and have been previously listed), and they will become immediately evident if encountered as they often produce chaotic orbits. If there are significant abnormalities in residuals, fits, or frequencies, then it can almost certainly be attributed to this effect. Slightly adjusting the orbit to move it from resonance or to increase the frequencies should solve any problems with commensurate frequencies.

The Nyquist-Shannon criteria requires at least two complete cycles of a frequency for acceptable data sampling. The apsidal frequency, which is usually the smallest, can be approximated by Equation (2.9). A clean approach would be to use the same time period for all orbits and pick a threshold frequency that all orbits must meet to be considered for use. A one year integration period is sufficient for analysis for frequencies on the order of 3.14×10^{-4} rad/TU, and it takes about three to four hours for computation. The frequencies will grow smaller as eccentricity increases, therefore, longer integration times are required for these test cases. An 8 year and 10 year integration will allow frequencies as low as

Table 3.1: Orbital Resonance due to Earth's Geopotential

Resonance	Orbital Period (sidereal time)	Semi-major Axis
1:1	24 hr	42,164.17 km
2:1	12 hr	26,561.76 km
3:1	8 hr	20,270.42 km
4:1	6 hr	16,732.86 km
5:1	4.8 hr	14,419.94 km
6:1	4 hr	12,769.56 km
7:1	3.429 hr	11,522.45 km
8:1	3 hr	10,541.04 km
9:1	2.667 hr	9,745.000 km
10:1	2.4 hr	9,083.994 km
11:1	2.18 hr	8,524.752 km
12:1	2 hr	8,044.320 km
13:1	1.846 hr	7,626.313 km
14:1	1.714 hr	7,258.689 km
15:1	1.6 hr	6,932.385 km

3.93×10^{-5} rad/TU and 3.14×10^{-5} rad/TU, respectively. Therefore, computational limits quickly impose themselves on orbit types since ω_3 can shrink beyond these limits as semi-major axis increases.

The following test cases were created based on considerations just discussed:

Test Case 0: Two orbits - nearly circular (see Figure 3.4).

This test case is the null case. It functions to replicate the results of previous research, analyze two different initial conditions, and note any changes between 0.01 eccentricity and 0.05 eccentricity.
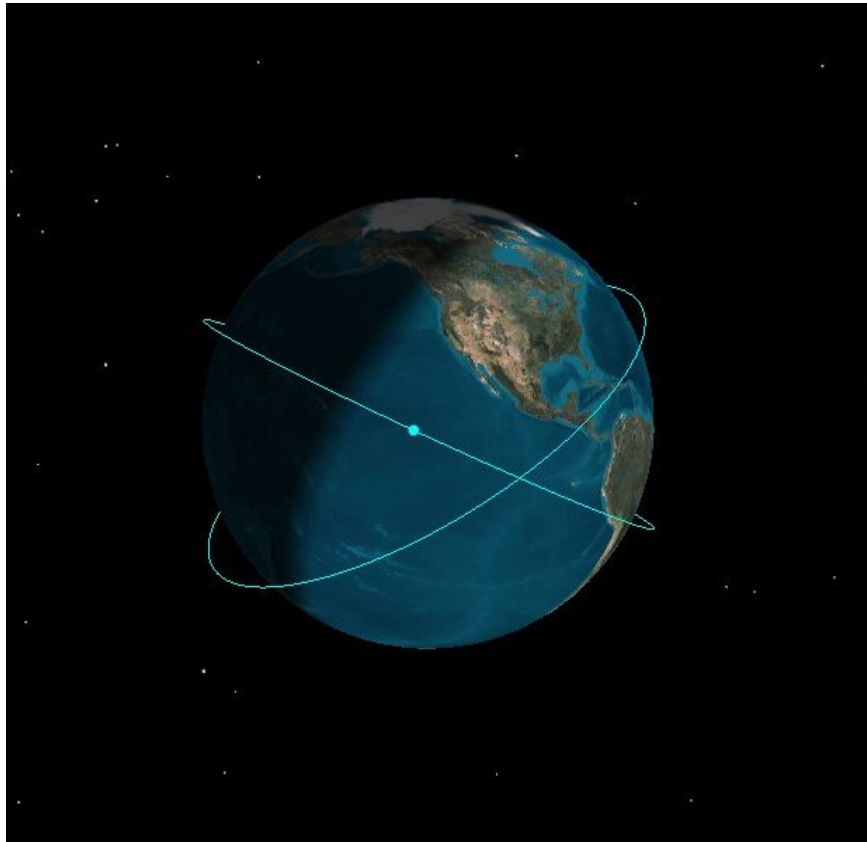

Figure 3.4: Test Case 0: Two orbits - nearly circular (generated by Systems Tool Kit)

Test Case 1: A series of orbits with increasing eccentricity holding perigee height constant (see Figure 3.5).

This test case is the best overall method to analyze orbits with increasing eccentricity for this research, because orbits that have a smaller semi-major axis have larger basis frequencies. This is advantageous, as smaller frequencies can pose a problem when acquiring the necessary cycles to meet the Nyquist-Shannon criteria. Analyzing bigger orbits is not impossible, but it typically requires a super efficient, refined code and lots of run time. Even in this particular test case, there may be problems/limitations with the larger orbits. It should be noted that TC2-7 is sitting on a resonance feature; this was done intentionally so that one may see the effects of such a placement.
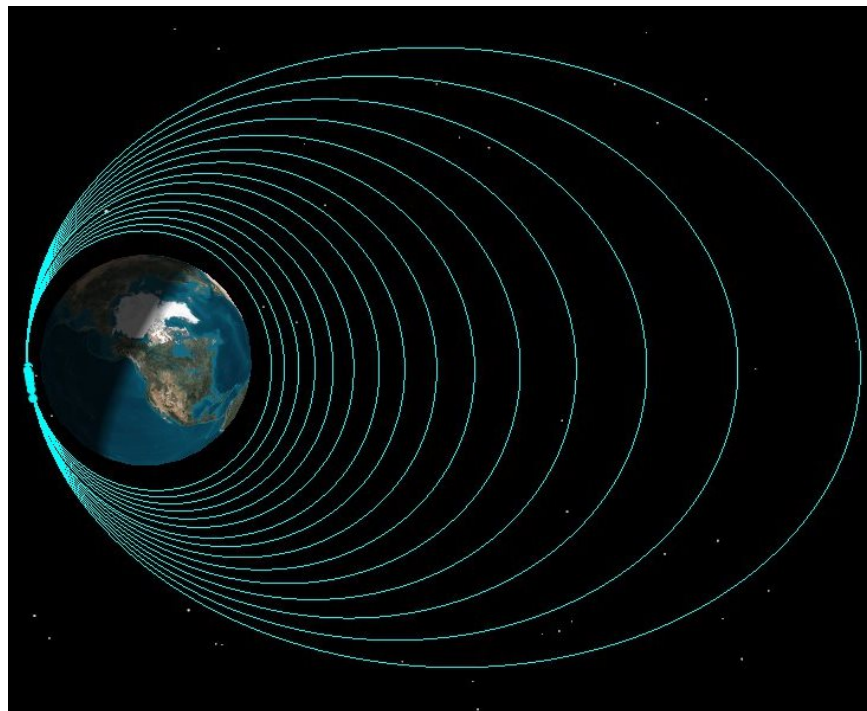
Figure 3.5: Test Case 1: Orbits with Increasing Eccentricity and Constant Perigee Height (generated by Systems Tool Kit)

Test Case X: A series of orbits with increasing eccentricity holding semi-major axis constant in the same plane (see Figure 3.6).

Test Case X would have essentially been a "nice to have," but it will not be included in this research. The large orbit sizes/small frequencies imposed fidelity restrictions that the software packages could not handle. It is only included here as a way to express a completeness in thought about eccentric orbits and to pose as a topic for future research.
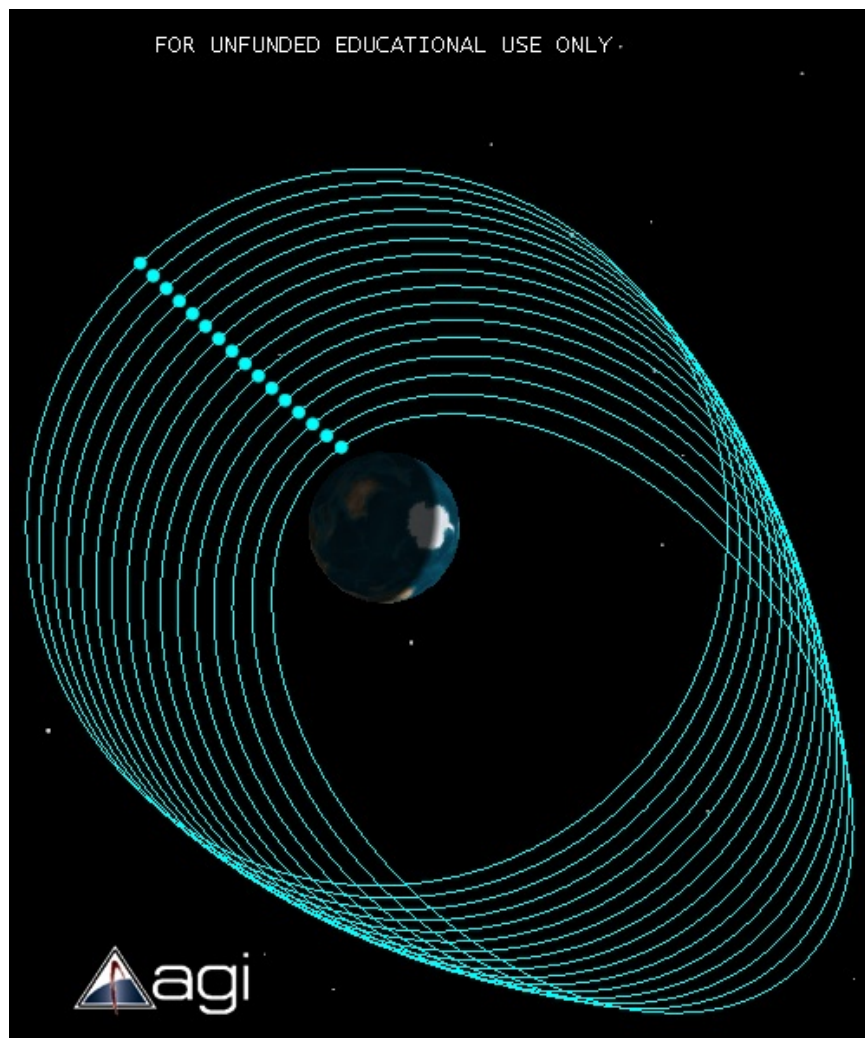

Figure 3.6: Test Case X: Orbits with Increasing Eccentricity and Constant Semi-Major Axis (generated by Systems Tool Kit)

3.2 Spectral Analysis

Jacques Laskar's spectral analysis method is the selected approach for constructing KAM tori. Though outlined in this section, a deeper study can be found within the following references: [14, 15]. Laskar's spectral analysis method begins with a Fourier transform of the data from the numerical integration. Careful consideration is needed when choosing the type of Fourier transform. The Fast Fourier Transform (FFT) is typically the "go-to" choice because of its speed and usefulness. Its processing speed is on the order of *N log(N)*, which makes it desirable for crunching through large amounts of data very quickly. This would seem especially attractive for the current research since a large amount of data is indeed being created. However, the FFT does not necessarily prove useful when used with long integration times, because the data most likely *is* a Fourier series as time goes to infinity. The end result would yield many frequency spikes with very large magnitudes. Instead, Laskar uses a finite Fourier transform, or Discrete Fourier Transform (DFT), with window functions. The DFT picks off the first Fourier coefficients by identifying the frequency with the highest magnitude. Applying a Newton-Rhapson algorithm to the area around an approximate frequency will identify the maxima, or main peak, among all the side lobes. This estimate is then refined by using Fourier integrals and the Hanning window function, after which it is subtracted out of the Fourier series [12]. Laskar uses the weighting, or windowing, function to account for "frequency leakage." "Leakage" occurs if the total time period does not contain an integer number of orbital periods. This process continues with each subsequent frequency component until all are identified. Many iterations of this process may be needed since the side lobes of adjacent spectral lines can contribute to and slightly skew the actual spectral line.

Laskar uses Equation (3.8) and Equation (3.9) as the finite Fourier transform and Hanning weighting function, respectively.

$$\phi(\omega) = \frac{1}{2T} \int_{T}^{T} q(t)e^{i\omega t}\chi_p(t/T)dt \tag{3.8}$$

$$\chi_p(t/T) = \frac{2^p(p!)^2}{(2p)!}\left(1 + cos\left(\frac{\pi t}{T}\right)\right) \tag{3.9}$$

The time interval is centered from [-T, T], and the window function is optimized such that it fades to zero when approaching the bound of this interval.

For a Hanning window function with a window power of $p=1$, Laskar has demonstrated that frequencies will converge at $1/T^4$, where the FFT converges at $1/T$. Increasing the window power, p, serves as a method to reduce "frequency leakage," but Laskar notes that accuracy decreases after $p=5$. For orbital data, the effect of increasing the window power is the rapid drop off of the side lobes around the main frequency peaks. Yet, a balance must be found, as increasing the window power will also widen the actual frequency peak, potentially decreasing the accuracy of the true frequency. A window power of $p = 2$ is suitable for the current research.

The general approach to extracting the Fourier series coefficients starts with Equation (3.10):

$$q(t) = \sum_j C_\mathbf{j} cos(\mathbf{j} \cdot \mathbf{\Omega} t) + S_\mathbf{j} sin(\mathbf{j} \cdot \mathbf{\Omega} t). \tag{3.10}$$

Once the approximate basis frequencies are known, the coefficients in Equation (3.10) are directly found through analysis of the Fourier transform via Equation (3.11), Equation (3.12), and Equation (3.13) [5]:

$$C_{(\mathbf{0,0,...,0})}\mathrm{N} = \mathfrak{R}\Phi(0), \tag{3.11}$$

$$C_\mathbf{j} = 2\mathfrak{R}\Phi(\Psi_\mathbf{j}), and \tag{3.12}$$

27

$$S_{\mathbf{j}} = -2\Im\Phi(\Psi_{\mathbf{j}}), \tag{3.13}$$

where $\Phi(\Psi_{\mathbf{j}})$ is the Fourier transform at $\Psi_{\mathbf{j}}$, and $\Re$ and $\Im$ are the real and imaginary parts of the Fourier transform. When this process is iterated, the refined results become more accurate. This is all that is needed to construct the torus, since the geometric structure of a torus is represented by a Fourier series with a set of basis frequencies (see Equation (3.14). The torus physical coordinates are easily found since new coordinates of the Hamiltonian increment linearly with time (see Equation (3.15)), and the momenta can be calculated from the Poincar$é$ integral invariants (see Equation (3.16)) [20].

$$\mathbf{q} = \sum_{j}(C_{\mathbf{j}} \cdot \mathbf{Q} + S_{\mathbf{j}} sin \mathbf{j} \cdot \mathbf{Q}) \tag{3.14}$$

$$Q_i(t) = \omega_i t + Q_{i0} \tag{3.15}$$

$$P_i = \frac{1}{2\pi} \int_0^{2\pi} \mathbf{p} \cdot \frac{\partial \mathbf{q}}{\partial Q_i} dQ_i \tag{3.16}$$

3.3 Model Validation

At the end of the day, the true measure of how well KAM tori theory applies to high eccentricity orbits are the residuals between the constructed torus and the integrated orbit. The smaller the root mean squared residual distances, the better the fit. Wiesel has already shown that it is possible to have residuals as small as five meters over a ten year period for orbits with an eccentricity near zero [20]. Assuming these higher eccentricity orbits are indeed a KAM torus, possible sources of error can lie either within the integrator or in determining the exact basis frequencies.

IV. Results

This chapter is organized first by test case and then by orbit type. A detailed analysis is made for each orbit type, and a brief overall summary for all the data is provided at the end of this chapter. The following information can be found for each test case, either in this section or in the appendices.

1. Test case analysis

2. A list of the orbital parameters for that particular orbit.

3. The fundamental basis frequencies from the KAM model.

4. The position residual between the integrated data set and the KAM model.

5. The Hamiltonian error from the integrated data set (Appendix A).

6. The frequency residual between the integrated data set and the KAM model (Appendix B).

Each test case and simulation was run with the following settings:

- Hanning window: 2

- Order of earth's geopotential: 20x20

- Frequency Fourier series summation limits $(\omega_1, \omega_2, \omega_3)$: (6,10,6) for TC0-1 and TC0-2; (8,14,8) for TC1-1,TC1-2,TC1-3; (17,10,3) for all others

- Spectral lines: 10 (see Table 4)

Table 4.1: Spectral Lines

Coordinate	Multiples of ω_1	Multiples of ω_2	Multiples of ω_3
1	1	1	1
2	1	1	1
1	1	-1	1
2	1	-1	1
3	1	0	1
1	2	1	1
2	2	1	1
1	2	-1	1
2	2	-1	1
3	2	0	1

4.1   Test Case 0: *Nearly*-Circular 7,000km Orbits

4.1.1   Test Case 0-1 (TC0-1).

This test case will act as the baseline for comparison for the results of every other test case. This particular test case, TC0-1, is a good demonstration of what is actually possible when applying a KAM torus model to orbit applications. TC0-1 was run over the course of 1 year, and it is similar to the orbit type that Wiesel demonstrated satellite prediction capability to a high level of accuracy and fidelity. This research shows very similar results, thereby corroborating Wiesel's findings and creating a baseline for this research.

4.1.1.1   Test Case Analysis.

There are no noticeable residual frequencies "standing out" above the rest in Figure 4.1, and, in fact, their magnitudes are all quite "small". This means that most of the dynamics have been captured by the three basis frequencies. This is further confirmed by looking at the position residuals and seeing it hover around 1.2 meter error (Figure 4.2).

Therefore, this test case accurately reproduces the 20x20 geopotential integrated solution with 1-2 *meter* position error over the span of an entire year. This, of course, does not take into account air drag or third body effects, however, the predictive accuracy of the KAM model is extremely promising and should not be overlooked for real-world satellite applications. A final note, the Hamiltonian error during the integration stays between 8×10^{-13} and 1^{-13}, removing any cause for concern of errors in the integration data itself (see Chapter A Figure A.1).

4.1.1.2 Orbital Parameters.

Table 4.1.1.2 shows the orbital parameters for TC0-1:

Table 4.2: TC0-1 Orbital Parameters

Integration Time and Orbital Elements	Values
Integration Time	1 year
Semi-major Axis	7,000 km
Eccentricity	0.01
Inclination	28.5 deg
Right Ascension of Ascending Node	100 deg
Argument of Perigee	100 deg
True Anomaly	45 deg

4.1.1.3 Basis Frequencies.

Table 4.1.1.3 holds the basis frequencies found by the KAM model.

Table 4.3: TC0-1 Basis Frequencies

Fundamental Frequency	KAM Frequency (rad/TU)	Goodness of Fit
ω_1	8.70666879297384e-001	6×10^{-13}
ω_2	-5.98694362109920e-002	6×10^{-13}
ω_3	1.68577168298212e-003	6×10^{-13}

4.1.1.4 Residuals.

Figure 4.1 shows the frequency residuals between the integrated data set and the KAM model, and Figure 4.2 shows the position residuals.
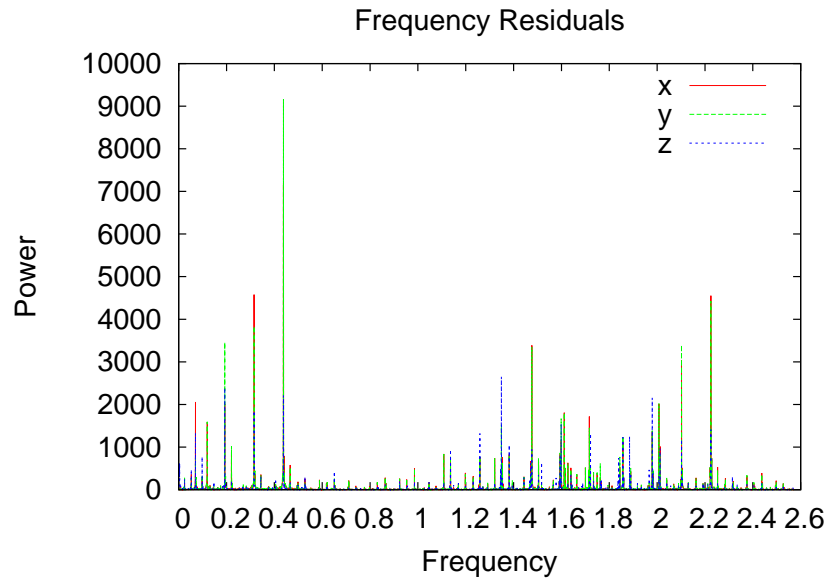

Figure 4.1: TC0-1 Frequency Residuals (1-year, a = 7,000 km, e = 0.01, i = 28.5 deg)
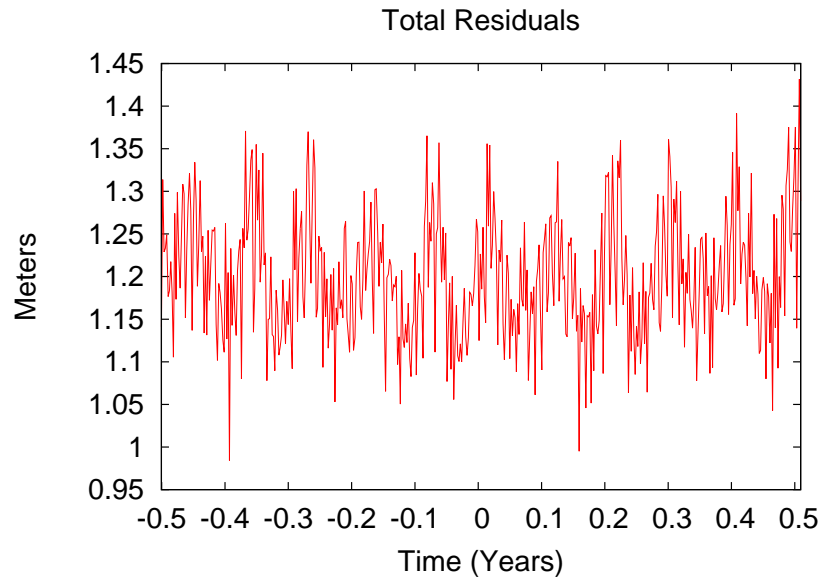
Figure 4.2: TC0-1 Position Residuals (1-year, a = 7,000 km, e = 0.01, i = 28.5 deg)

4.1.2   Test Case 0-2 (TC0-2).

Similar to the previous test case, TC0-2 attempts to use slightly different initial conditions to test convergence. At the same time, the eccentricity for TC0-2 is raised from TC0-1 from 0.01 to 0.05.

4.1.2.1   Test Case Analysis.

Again, there are no dominant residual frequencies, so the position error should be fairly small, and it is. Notice in Figure 4.4 that the position error is between 1.6 and 3 meters. The Hamiltonian error is actually smaller than it was in TC0-1, this time ranging between 4.5×10^{-13} and 5×10^{-14} (see Chapter A Figure A.2), yet the position residuals are a tiny bit larger. This turns out to be a common finding in the results, that when eccentricity (and indirectly semi-major axis) increases, the residuals also increase. It may also be linked to the basis frequencies *shrinking* as eccentricity and semi-major axis increase. But, in this particular test case, the KAM model still predicts extremely well. Another important characteristic to notice in Figure 4.4 is the sinusoidal, periodic nature of the residuals. This

33

indicates that higher order harmonics of the frequencies are not accounted for in the model. These higher order harmonics become a more dominant source of error as eccentricity increases.

4.1.2.2 Orbital Parameters.

Table 4.4: TC0-2 Orbital Parameters

Integration Time and Orbital Elements	Values
Integration Time	1 year
Semi-major Axis	7,049.5 km
Eccentricity	0.05
Inclination	30 deg
Right Ascension of Ascending Node	261.72 deg
Argument of Perigee	141.41 deg
True Anomaly	94.147 deg

4.1.2.3 Basis Frequencies.

Table 4.5: TC0-2 Basis Frequencies

Fundamental Frequency	KAM Frequency (rad/TU)	Goodness of Fit
ω_1	8.61166268317812e-001	1×10^{-13}
ω_2	-5.98330343009343e-002	1×10^{-13}
ω_3	1.58570923267964e-003	1×10^{-13}

4.1.2.4 Residuals.
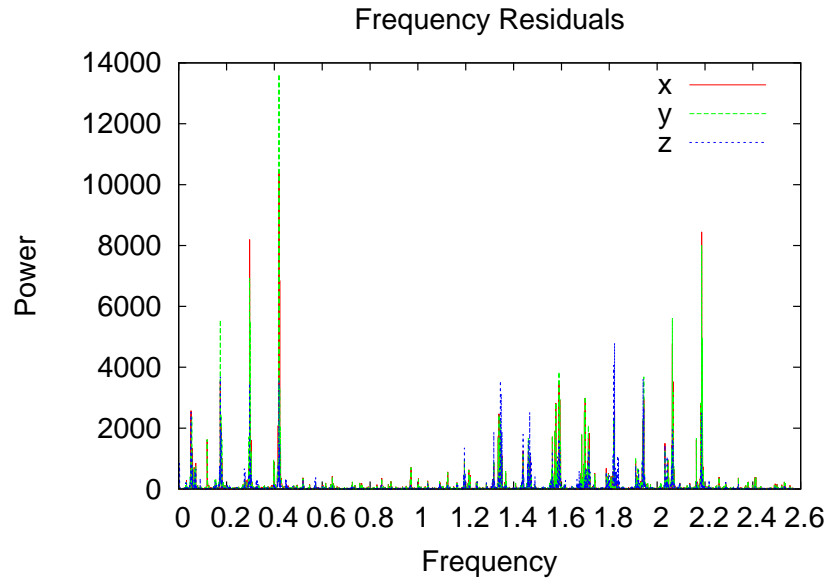
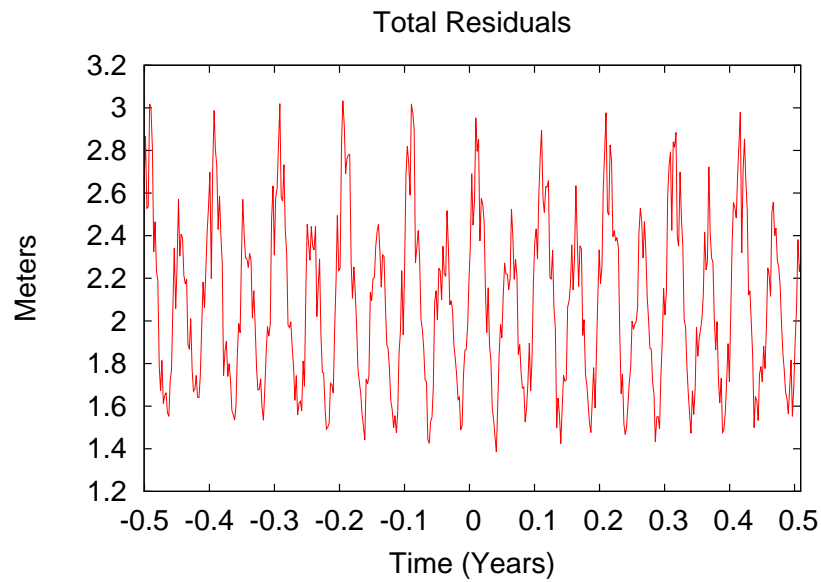Figure 4.3: TC0-2 FFT Residuals (1-year, a = 7,049.5 km, e = 0.05, i = 30 deg)

Figure 4.4: TC0-2 Position Residuals (1-year, a = 7,049.5 km, e = 0.05, i = 30 deg)

4.2 Test Case 1: Increasing Eccentric Orbits

This test case is the basis for the KAM theory model and eccentric orbit research. The goal is to gradually increase eccentricity (holding perigee height constant) and see if the model residuals remain at or near the same levels as Test Case 1. Relevant questions to consider are:

1. Do residuals drop off slowly as eccentricity increases, and, if so, why?

2. Do residuals have a sharp drop as eccentricity increases? Is there an eccentricity that acts as a proverbial wall where the model is no longer viable past that point, and, if so, why?

3. Do the basis frequency fits decrease as eccentricity increases, and, if so, why?

4. Does Hamiltonian error ever become a factor?

After a summary of each orbit in this test case is presented, an overall summary that addresses the above questions can be found at the end of this chapter.

4.2.1 Test Case 1-1 (TC1-1).

This test case starts at 0.05 eccentricity, and Table 4.2.1.2 shows the new orbital initial conditions. There is no resonance feature at this particular height and inclination.

4.2.1.1 Test Case Analysis.

Because eccentricity is the same as TC0-2, one should expect similar results. In fact, we see a remarkable fit of the fundamental frequencies, Table 4.2.1.3, and an even tighter fit of the position residuals, Figure 4.5. These improvements in the basis frequency fits are directly attributable to a four year time interval instead of a one year time interval. This is because the increased data makes the existing basis frequencies (and their multiples) more pronounced. It is, then, much easier to find the local maximums when the most prominent spectral lines are clearly seen above other nearby peaks. Improvements in the position residuals are linked to two factors, however. First, increasing the fit of the basis frequencies does have a small effect. But, the greater effect (if the basis frequency fits

are already sufficiently small) is increasing/adjusting the number of terms included in the Fourier series expansion allowing for the inclusion of higher order frequency multiples. In this case, inclusion of these terms drives down the residuals to a greater degree, as the error induced by not including them can have a tens of meters to thousands of meters level of impact. Overall, this orbit type is almost identically a KAM torus. One other point of note; notice the linear growth after 2 years. This is indicative of the limits of double precision computing. That is, sometimes a single bit is lost off the edge of the product $\omega \times t$ when t is large and $\omega \times t$ is reduced modulo $2 \times \pi$.

4.2.1.2 Orbital Parameters.

Table 4.6: TC1-1 Orbital Parameters

Integration Time and Orbital Elements	Values
Integration Time	4 years
Semi-major Axis	7,894.74 km
Eccentricity	0.05
Inclination	30 deg
Right Ascension of Ascending Node	261.716 deg
Argument of Perigee	141.412 deg
True Anomaly	1.54321 deg

4.2.1.3 Basis Frequencies.

Table 4.7: TC1-1 Basis Frequencies

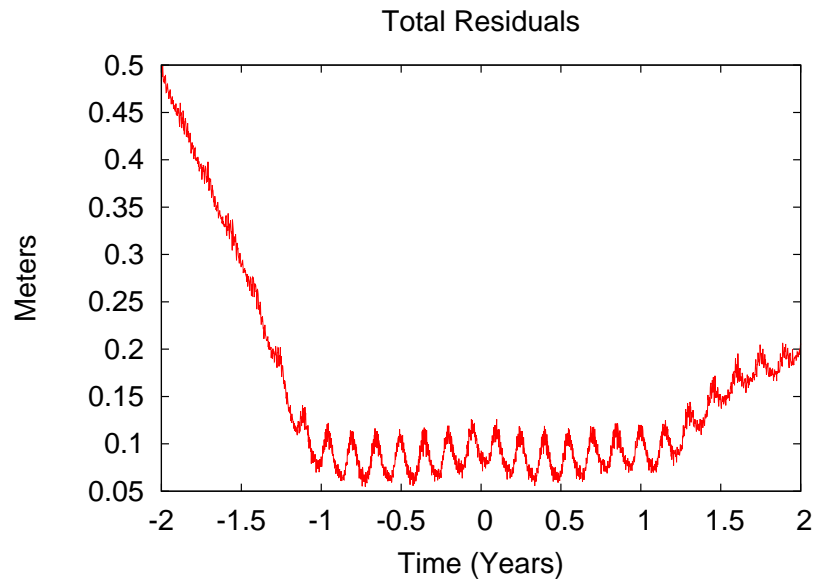| Fundamental Frequency	KAM Frequency (rad/TU)	Goodness of Fit
ω_1	7.26812125849350e-001	1×10^{-16}
ω_2	-5.95059837411420e-002	1×10^{-16}
ω_3	1.06716141007723e-003	1×10^{-16}

4.2.1.4 Residuals.

Figure 4.5: TC1-1 Position Residuals

4.2.2 Test Case 1-2 (TC1-2).

A simple pattern follows from here on through TC1-15 as eccentricity is increased by adding 0.05 while all other parameters remain constant save semi-major axis. Eccentricity is now 0.1.

4.2.2.1 Test Case Analysis.

Table 4.2.2.3 shows an impressive fit of the basis frequencies, and Figure 4.6 again demonstrates that the KAM model is capable of sub-meter level accuracy. This orbit type is also almost identically a KAM torus. And, as seen previously, there is still information not captured in the KAM model as evidenced by the periodic nature of the residuals.

4.2.2.2 Orbital Parameters.

Table 4.8: TC1-2 Orbital Parameters

Integration Time and Orbital Elements	Values
Integration Time	4 years
Semi-major Axis	8,333.34 km
Eccentricity	0.10
Inclination	30 deg
Right Ascension of Ascending Node	261.716 deg
Argument of Perigee	141.412 deg
True Anomaly	1.54321 deg

4.2.2.3 Basis Frequencies.

Table 4.9: TC1-2 Basis Frequencies

| Fundamental Frequency	KAM Frequency (rad/TU)	Goodness of Fit
ω_1	6.70228683577018e-001	1×10^{-16}
ω_2	-5.93983833551193e-002	1×10^{-16}
ω_3	8.96409693408984e-004	1×10^{-15}

4.2.2.4   Residuals.
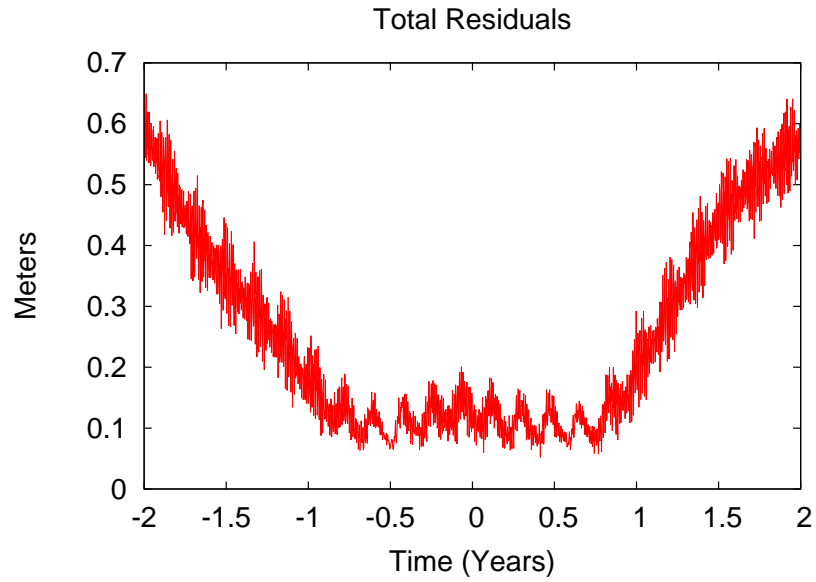
Figure 4.6: TC1-2 Position Residuals

4.2.3   Test Case 1-3 (TC1-3).

Eccentricity is now 0.15.

4.2.3.1   Test Case Analysis.

Very similar to TC1-1 and TC1-2, the basis frequencies for TC1-3 (see Table 4.2.3.3) fit quite well, and Figure 4.7 shows that, *again*, there is sub-meter level accuracy. This orbit type is also almost identically a KAM torus.

4.2.3.2 Orbital Parameters.

Table 4.10: TC1-3 Orbital Parameters

Integration Time and Orbital Elements	Values
Integration Time	4 years
Semi-major Axis	8,823.55 km
Eccentricity	0.15
Inclination	30 deg
Right Ascension of Ascending Node	261.716 deg
Argument of Perigee	141.412 deg
True Anomaly	1.54321 deg

4.2.3.3 Basis Frequencies.

Table 4.11: TC1-3 Basis Frequencies

| Fundamental Frequency	KAM Frequency (rad/TU)	Goodness of Fit
ω_1	6.15194193460185e-001	1×10^{-15}
ω_2	-5.93077891050983e-002	1×10^{-15}
ω_3	7.52634053553081e-004	1×10^{-15}

4.2.3.4 Residuals.
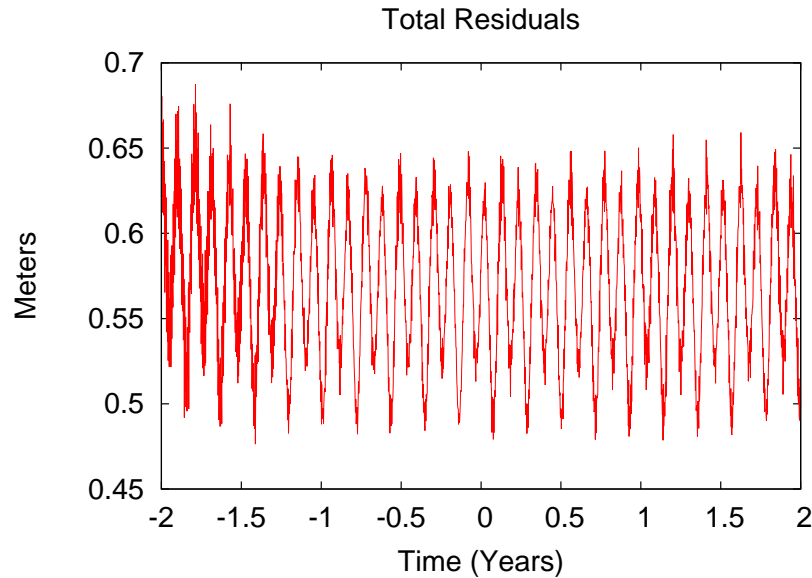
Figure 4.7: TC1-3 Position Residuals

4.2.4 Test Case 1-4 (TC1-4).

Eccentricity is now 0.2.

4.2.4.1 Test Case Analysis.

This is the first test case in which the residuals begins to trend downward. However, it is not a dramatic downward trend (at least not at this point). There is a slight drop in the basis frequencies; the trend has thus far gone from 10^{-16} to 10^{-15} and now to 10^{-14}. This trend can be simply explained. As eccentricity increases, all frequency multiples begin to become more significant, since most geopotential terms scale by eccentricity. Because these once small frequency terms are now growing, their "peaks" (which are really lobes) are contributing to the "peaks" (or lobes) of their neighbors as well. This can offset the local maximum just slightly enough to slowly decrease the fit over time. However, increasing the time period from four years to something much higher, say eight, twelve, or even

42

sixteen years, would serve as a way to increase the fit of these frequencies. Due to software limitations, this research was limited to a four year fit, therefore, this downward trend will continue as eccentricity rises. Despite this shortcoming, Figure 4.8 shows residuals on the order of meters to tens of meters, which still indicate that this orbit type is a KAM torus. Both double precision limits and periodic nature of the residuals are seen in this test case as well (see previous analysis for explanation).

4.2.4.2 Orbital Parameters.

Table 4.12: TC1-4 Orbital Parameters

Integration Time and Orbital Elements	Values
Integration Time	4 years
Semi-major Axis	9,375 km
Eccentricity	0.20
Inclination	30 deg
Right Ascension of Ascending Node	261.716 deg
Argument of Perigee	141.412 deg
True Anomaly	1.54321 deg

4.2.4.3 Basis Frequencies.

Table 4.13: TC1-4 Basis Frequencies

Fundamental Frequency	KAM Frequency (rad/TU)	Goodness of Fit
ω_1	5.61758109567672e-001	1×10^{-15}
ω_2	-5.92311866057489e-002	1×10^{-14}
ω_3	6.31056599189606e-004	1×10^{-14}

43
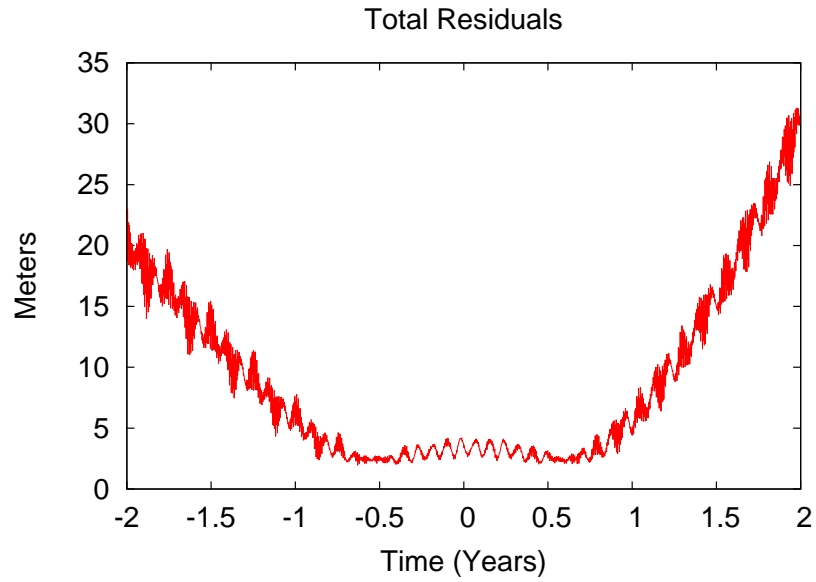
4.2.4.4 Residuals.
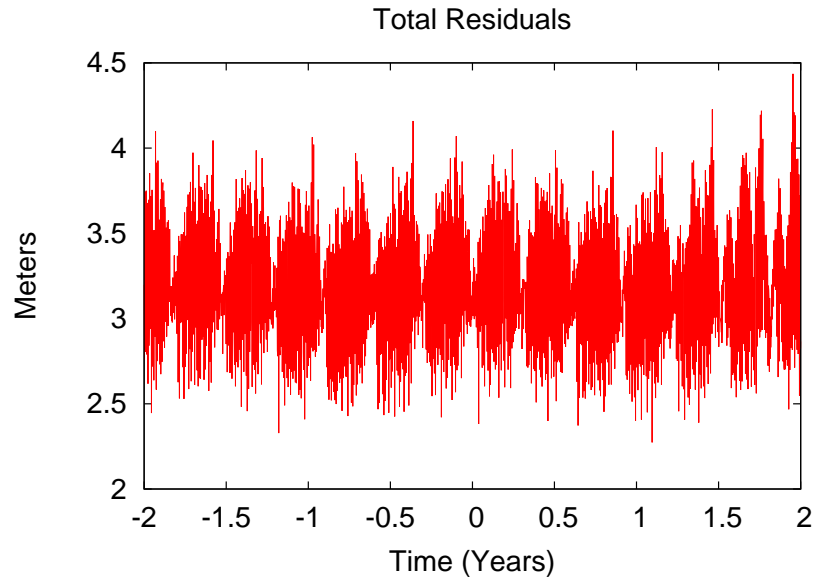

Figure 4.8: TC1-4 Position Residuals

4.2.5 Test Case 1-5 (TC1-5).

Eccentricity is now 0.25.

4.2.5.1 Test Case Analysis.

The downward trend of the basis frequencies fit continues, but the position residuals are still at an impressive 3 meter accuracy. Therefore, this orbit type is also close to a KAM torus.

4.2.5.2   Orbital Parameters.

Table 4.14: TC1-5 Orbital Parameters

Integration Time and Orbital Elements	Values
Integration Time	4 years
Semi-major Axis	10,000 km
Eccentricity	0.25
Inclination	30 deg
Right Ascension of Ascending Node	261.716 deg
Argument of Perigee	141.412 deg
True Anomaly	1.54321 deg

4.2.5.3   Basis Frequencies.

Table 4.15: TC1-5 Basis Frequencies

Fundamental Frequency	KAM Frequency (rad/TU)	Goodness of Fit
ω_1	5.09963957456222e-001	1×10^{-14}
ω_2	-5.91661723590575e-002	1×10^{-14}
ω_3	5.27866773079033e-004	1×10^{-13}

4.2.5.4   Residuals.

Figure 4.9: TC1-5 Position Residuals

4.2.6   Test Case 1-6 (TC1-6).

Eccentricity is now 0.3.

4.2.6.1   Test Case Analysis.

The basis frequency fit roughly the same as in TC1-5, but, the position residuals have now dropped to 10 meter accuracy. This is because a second software limitation has been reached. That is, the maximum amount of Fourier series expansion terms that the software can handle has been met, and achieving meter level accuracy would require the inclusion of more terms. Since this isn't possible in the current research, a downward trend of position residuals begins here. Even so, this orbit type still closely resembles a KAM torus.

4.2.6.2 Orbital Parameters.

Table 4.16: TC1-6 Orbital Parameters

Integration Time and Orbital Elements	Values
Integration Time	4 years
Semi-major Axis	10,714.3 km
Eccentricity	0.30
Inclination	30 deg
Right Ascension of Ascending Node	261.716 deg
Argument of Perigee	141.412 deg
True Anomaly	1.54321 deg

4.2.6.3 Basis Frequencies.

Table 4.17: TC1-6 Basis Frequencies

Fundamental Frequency	KAM Frequency (rad/TU)	Goodness of Fit
ω_1	4.59866930816288e-001	1×10^{-14}
ω_2	-5.91108326057240e-002	1×10^{-14}
ω_3	4.40029936057407e-004	1×10^{-13}

4.2.6.4   Residuals.
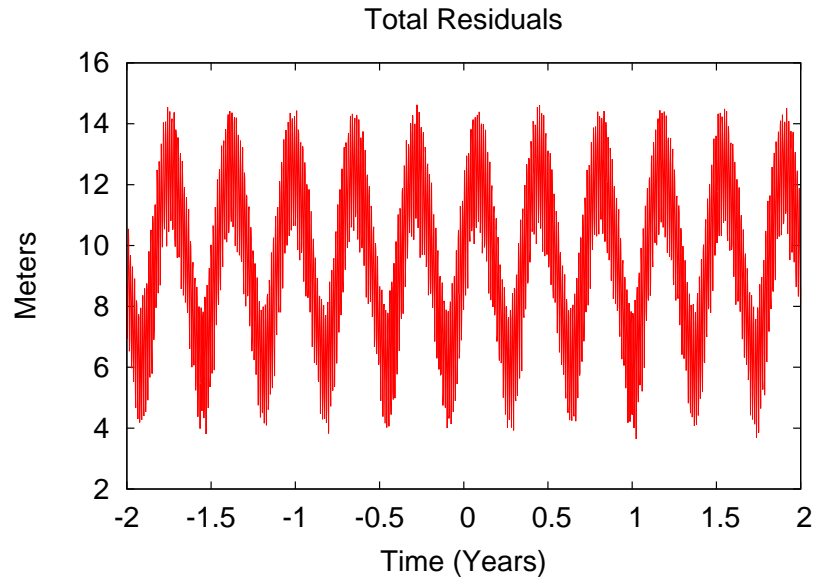
Figure 4.10: TC1-6 Position Residuals

4.2.7   Test Case 1-7 (TC1-7).

Eccentricity is now 0.35. This orbit type lies on a resonance feature.

4.2.7.1   Test Case Analysis.

The purpose of this orbit is to show the effect that resonance has on the KAM torus model. Notice in Table 4.2.7.3 that the basis frequency fit drops to an abysmal level. Strictly as a result of the bad fit, the position residuals shoot up to *3.67 million* meter accuracy (see Figure 4.11). Though the results do not indicate a KAM torus, notice that the residuals are about an earth radius in length. The fit for this orbit is near the earth, just not a torus. This is a caution to be careful near resonance!

48

4.2.7.2 Orbital Parameters.

Table 4.18: TC1-7 Orbital Parameters

Integration Time and Orbital Elements	Values
Integration Time	4 years
Semi-major Axis	11,638.5 km
Eccentricity	0.35
Inclination	30 deg
Right Ascension of Ascending Node	261.716 deg
Argument of Perigee	141.412 deg
True Anomaly	1.54321 deg

4.2.7.3 Basis Frequencies.

Table 4.19: TC1-7 Basis Frequencies

Fundamental Frequency	KAM Frequency (rad/TU)	Goodness of Fit
ω_1	4.07425742649731e-001	1×10^{-7}
ω_2	-5.90569629903617e-002	1×10^{-7}
ω_3	-8.43488328402309e-004	1×10^{-7}

4.2.7.4   Residuals.
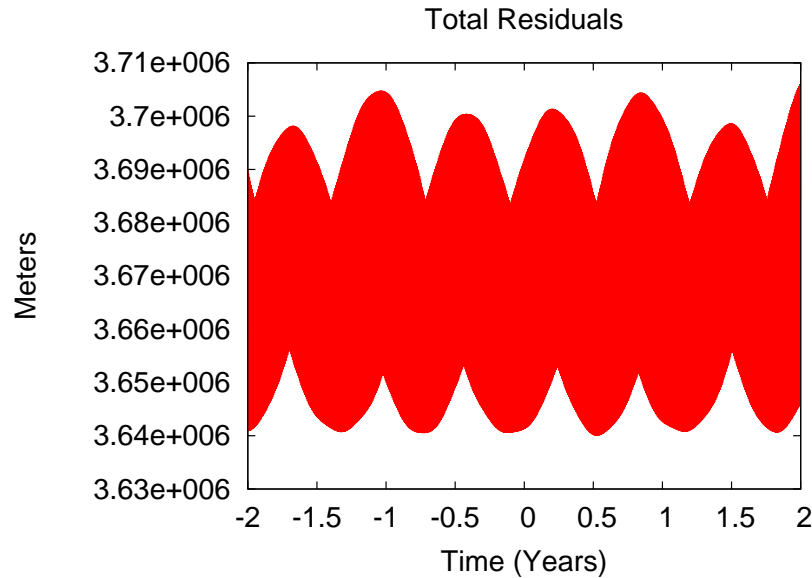
Figure 4.11: TC1-7 Position Residuals

4.2.8   Test Case 1-8 (TC1-8) Through Test Case 1-12 (TC1-12).

These orbit types all show similar trends, therefore, they will be analyzed together. Refer to the orbital parameters for the eccentricities of each orbit type.

4.2.8.1   Test Case Analysis.

These five orbit types show an exponential increase in residual growth as eccentricity scales larger. This is not due to goodness of fit error, since all are around 10^{-11} or higher, which is similar to previous orbit types. The residual growth here is due to increasing error in the Fourier series expansion terms and not being able to account for this in the software. The software is memory limited due to the way it stores values from these terms in arrays; they grow past a manageable size for normal computing when extra Fourier expansion terms are added. TC1-8, TC1-9, and TC1-10 clearly resemble KAM tori as the residuals

are still small (10s of meters). The data suggests that TC1-11 and TC1-12 also resemble KAM tori, however, a code rewrite is required to actually demonstrate this.

4.2.8.2 Orbital Parameters.

Table 4.20: TC1-8 Orbital Parameters

Integration Time and Orbital Elements	Values
Integration Time	4 years
Semi-major Axis	12,500 km
Eccentricity	0.40
Inclination	30 deg
Right Ascension of Ascending Node	261.716 deg
Argument of Perigee	141.412 deg
True Anomaly	1.54321 deg

Table 4.21: TC1-9 Orbital Parameters

Integration Time and Orbital Elements	Values
Integration Time	4 years
Semi-major Axis	13,636.4 km
Eccentricity	0.45
Inclination	30 deg
Right Ascension of Ascending Node	261.716 deg
Argument of Perigee	141.412 deg
True Anomaly	1.54321 deg

Table 4.22: TC1-10 Orbital Parameters

Integration Time and Orbital Elements	Values
Integration Time	4 years
Semi-major Axis	15,000 km
Eccentricity	0.50
Inclination	30 deg
Right Ascension of Ascending Node	261.716 deg
Argument of Perigee	141.412 deg
True Anomaly	1.54321 deg

Table 4.23: TC1-11 Orbital Parameters

Integration Time and Orbital Elements	Values
Integration Time	4 years
Semi-major Axis	16,666.6 km
Eccentricity	0.55
Inclination	30 deg
Right Ascension of Ascending Node	261.716 deg
Argument of Perigee	141.412 deg
True Anomaly	1.54321 deg

Table 4.24: TC1-12 Orbital Parameters

Integration Time and Orbital Elements	Values
Integration Time	4 years
Semi-major Axis	18,750 km
Eccentricity	0.60
Inclination	30 deg
Right Ascension of Ascending Node	261.716 deg
Argument of Perigee	141.412 deg
True Anomaly	1.54321 deg

4.2.8.3 Basis Frequencies.

Table 4.25: TC1-8 Basis Frequencies

Fundamental Frequency	KAM Frequency (rad/TU)	Goodness of Fit
ω_1	3.65014634255894e-001	1×10^{-12}
ω_2	-5.90232904034811e-002	1×10^{-12}
ω_3	3.01080387980157e-004	1×10^{-12}

Table 4.26: TC1-9 Basis Frequencies

Fundamental Frequency	KAM Frequency (rad/TU)	Goodness of Fit
ω_1	3.20398027800353e-001	1×10^{-12}
ω_2	-5.89888029375723e-002	1×10^{-12}
ω_3	2.46339635450177e-004	1×10^{-12}

Table 4.27: TC1-10 Basis Frequencies

Fundamental Frequency	KAM Frequency (rad/TU)	Goodness of Fit
ω_1	2.77766334373961e-001	1×10^{-12}
ω_2	-5.89593200868168e-002	1×10^{-12}
ω_3	1.99544853012767e-004	1×10^{-11}

Table 4.28: TC1-11 Basis Frequencies

Fundamental Frequency	KAM Frequency (rad/TU)	Goodness of Fit
ω_1	2.37212024832835e-001	1×10^{-10}
ω_2	-5.89341418092880e-002	1×10^{-10}
ω_3	1.59586266806677e-004	1×10^{-10}

Table 4.29: TC1-12 Basis Frequencies

Fundamental Frequency	KAM Frequency (rad/TU)	Goodness of Fit
ω_1	1.98854533213505e-001	1×10^{-11}
ω_2	-5.89126932326301e-002	1×10^{-11}
ω_3	1.25539449022050e-004	1×10^{-10}

Total Residuals
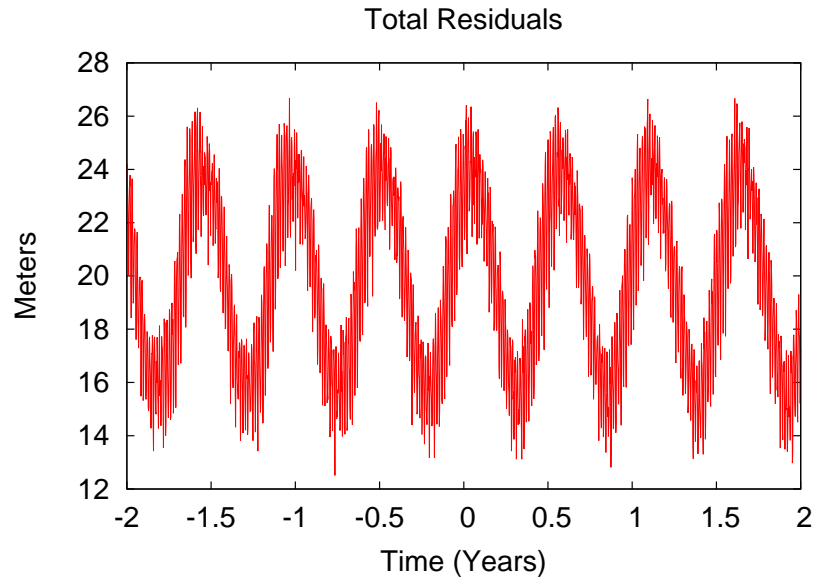
Figure 4.12: TC1-8 Position Residuals

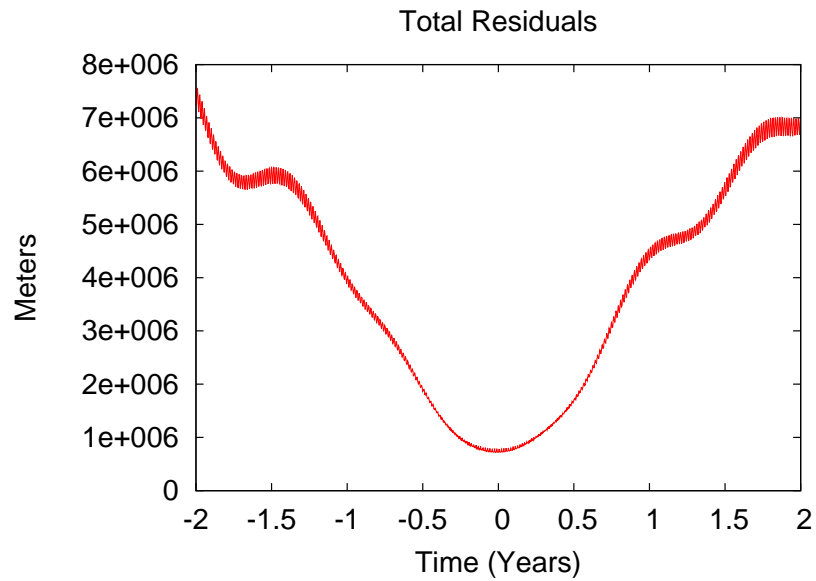## Total Residuals
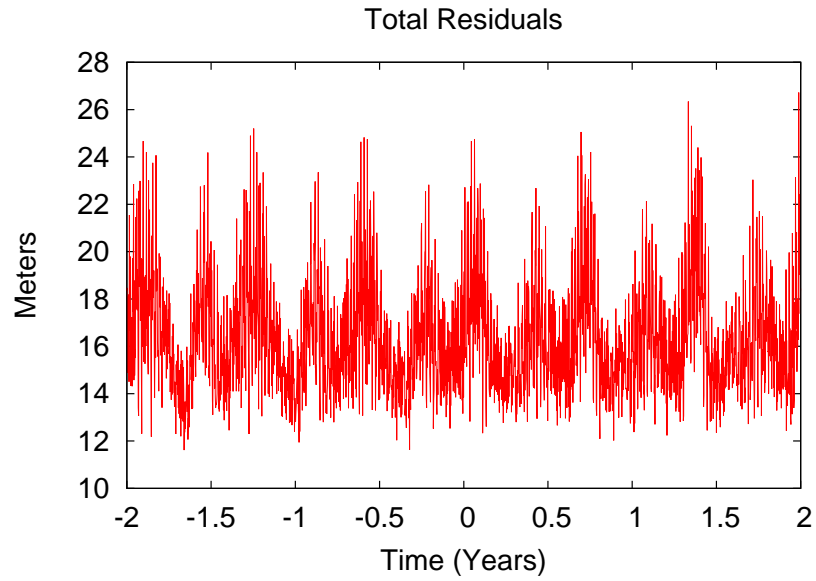
Figure 4.13: TC1-9 Position Residuals
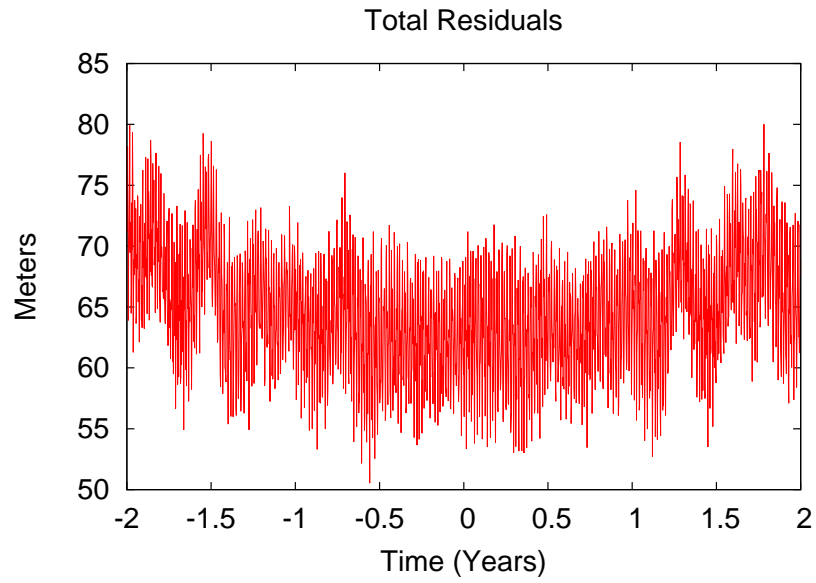
Figure 4.14: TC1-10 Position Residuals
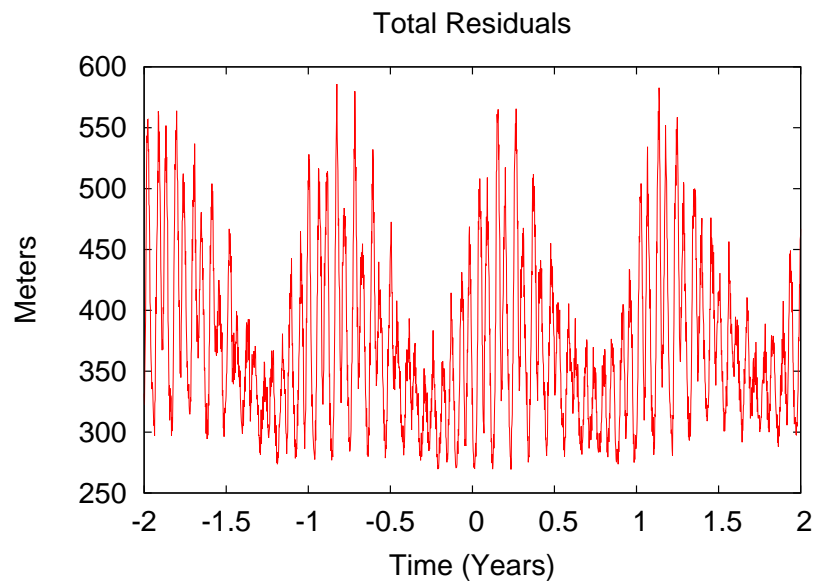
Figure 4.15: TC1-11 Position Residuals
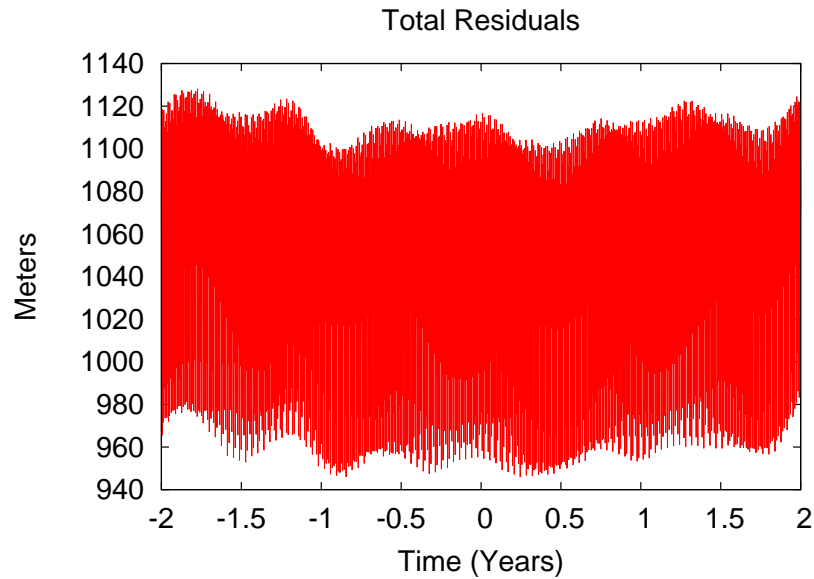
Figure 4.16: TC1-12 Position Residuals

4.2.9   Test Case 1-13 (TC1-13) Through Test Case 1-15 (TC1-15).

These orbit types all show similar trends, therefore, they will be analyzed together. Refer to the orbital parameters for the eccentricities of each orbit type.

4.2.9.1   Test Case Analysis.

These final three cases are trending to show that the KAM model with the current software ends here. It is clear that the goodness of fit error has dropped below acceptable levels, and the Fourier series expansion term error has grown considerably. As discussed before, enhanced software and longer integrations should be able to produce meter level residuals. Notice, also, the smaller frequencies. *Any* orbital data with frequencies on this order will have difficulty converging to a KAM torus fit due to limitations of the Nyquist-Shannon Theorem.

4.2.9.2 *Orbital Parameters.*

Table 4.30: TC1-13 Orbital Parameters

Integration Time and Orbital Elements	Values
Integration Time	4 years
Semi-major Axis	21,428.5 km
Eccentricity	0.65
Inclination	30 deg
Right Ascension of Ascending Node	261.716 deg
Argument of Perigee	141.412 deg
True Anomaly	1.54321 deg

Table 4.31: TC1-14 Orbital Parameters

Integration Time and Orbital Elements	Values
Integration Time	4 years
Semi-major Axis	25,000 km
Eccentricity	0.70
Inclination	30 deg
Right Ascension of Ascending Node	261.716 deg
Argument of Perigee	141.412 deg
True Anomaly	1.54321 deg

Table 4.32: TC1-15 Orbital Parameters

Integration Time and Orbital Elements	Values
Integration Time	4 years
Semi-major Axis	30,000 km
Eccentricity	0.75
Inclination	30 deg
Right Ascension of Ascending Node	261.716 deg
Argument of Perigee	141.412 deg
True Anomaly	1.54321 deg

4.2.9.3 Basis Frequencies.

Table 4.33: TC1-13 Basis Frequencies

Fundamental Frequency	KAM Frequency (rad/TU)	Goodness of Fit
ω_1	1.62930470077731e-001	1×10^{-6}
ω_2	-5.87922033105468e-002	1×10^{-6}
ω_3	-1.10629870846868e-004	1×10^{-5}

Table 4.34: TC1-14 Basis Frequencies

Fundamental Frequency	KAM Frequency (rad/TU)	Goodness of Fit
ω_1	1.29273816222032e-001	1×10^{-6}
ω_2	-5.88068248239637e-002	1×10^{-6}
ω_3	-5.01544398989751e-006	1×10^{-5}

Table 4.35: TC1-15 Basis Frequencies

Fundamental Frequency	KAM Frequency (rad/TU)	Goodness of Fit
ω_1	9.84228934385216e-002	1×10^{-6}
ω_2	-5.88148526461276e-002	1×10^{-6}
ω_3	-1.89849053721436e-005	1×10^{-5}

4.2.9.4   Residuals.

Figure 4.17: TC1-13 Position Residuals
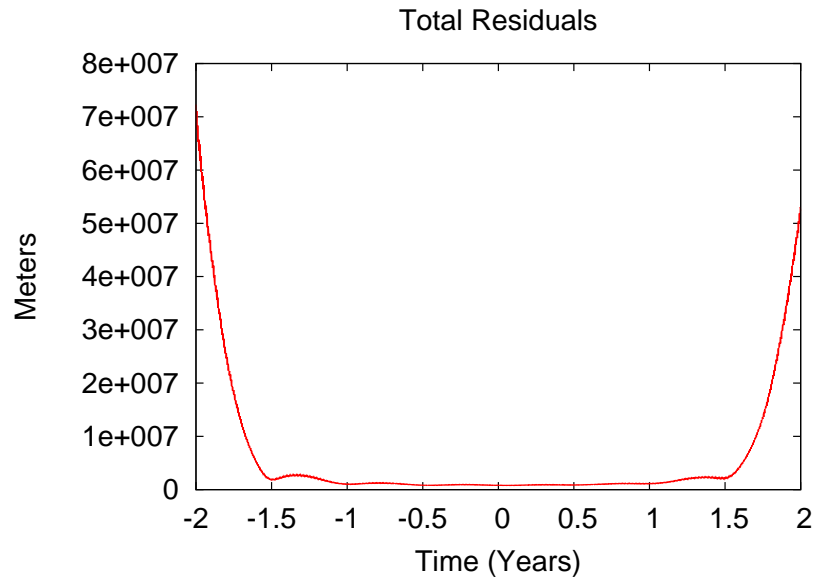
Figure 4.18: TC1-14 Position Residuals
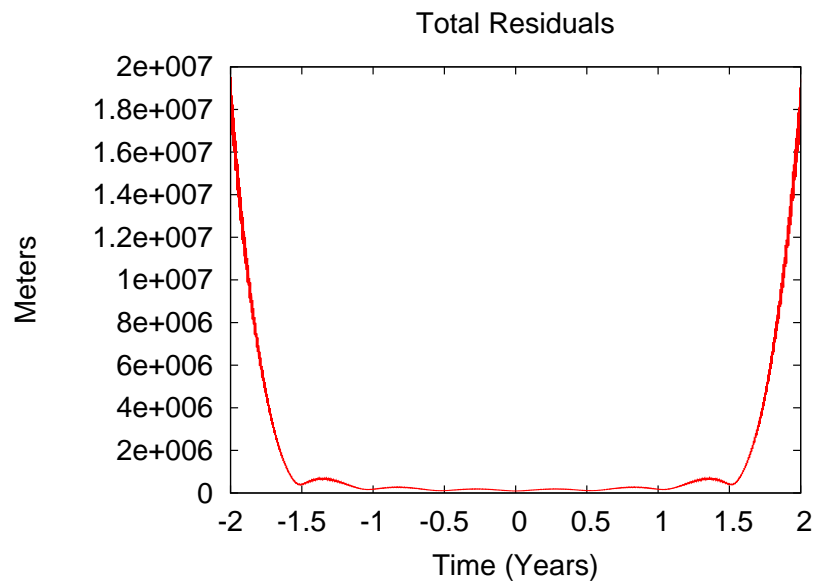
Figure 4.19: TC1-15 Position Residuals

61

4.3   Results Summary

TC1-1 through TC1-10 (eccentricity 0.05 through 0.5) showed a remarkable resemblance to a KAM torus for these orbit types. But, because of software limitations, more and more error was introduced as eccentricity increased because of decreasing frequencies residing outside of the Nyquist-Shannon Theorem limits. This resulted in both goodness of fit error and position residual error. Increase error in Fourier series expansion terms also contributed to the position residual error. Therefore, TC1-11 through TC1-15 do not match closely with the KAM model. The trend of data, however, suggests that these orbit types may actually be KAM tori. It would take an enhanced code and longer integrations (on the order of weeks real run time) to demonstrate this.

V.   Conclusions

KAM tori theory as it applies to orbits is still vastly unexplored. This research has focused on determining the viability of the theory as eccentricity increases among a set orbit type. In order to see the effect of solely the earth's geopotential, unhindered from third-body perturbation, a baseline set of comparison position data was created with a Hamming integrator and a 20x20 order geopotential model. Laskar's spectral method gives the ability to find a set of basis frequencies from a Fourier series, and those basis frequencies are then able to yield position data for a torus. A comparison of the torus position data and the integrated position data produced residuals, and a detailed analysis of this information has led to some clear limitations, conclusions, and recommendations.

5.1   Limitations

Several limitations have surfaced during the course of the research:

- The biggest limitation of these results is that the only satellite perturbation captured in the analysis is the earth's geopotential. Further research is being conducted concerning the effects of air drag and third-body perturbations on KAM theory, but all results from this research should be looked at through a limited perturbation lens.
- As seen in TC1-7, KAM theory for earth satellites does not hold up for orbits located in resonance or for orbits near 0 degrees inclination or the critical inclination. Resonance is an indication that the basis frequencies are nearly or exactly commensurate, and orbits that are equatorial or at the critical inclination cause a frequency to drop out altogether, ω_2 and ω_3 respectively.
- The code/software for this research, while robust in its own right, was pushed to its limits. This imposed limitations on the fidelity of the data for higher eccentricity orbits. The maximum time span that the software could process was about four

years, and the maximum number of Fourier series expansion terms that could be included was about 30 (total, all degrees of freedom). Effects from the time span limitation could be seen gradually throughout the data as the goodness of fit for the basis frequency dropped consistently, most evident in TC1-13 through TC1-15 (see Table 4.2.9.3, Table 4.2.9.3, and Table 4.2.9.3. Because of the time span limitation, the software was unable to fit the data with any precision at all for these three orbit types. The time span limitation itself is related to the decreasing basis frequencies (as eccentricity rises) moving outside the bounds of the Nyquist-Shannon Theorem requirements. An 8, 12, or possibly even a 16 year integration/fit would solve this issue, but it would require a re-write of the code to address memory storage issues when fitting data. Effects from the Fourier series expansion term limitation were also seen throughout the data. In fact, this was the primary cause for the initial *gradual* increase in position residuals as eccentricity increased (TC1-1 through TC1-8) and the *exponential* increase in position residuals around TC1-9. The periodic, sinusoidal nature of the residuals also substantiates this claim. The root cause for this growth is that the terms in the earth's geopotential scale greatly with eccentricity. Therefore, when converted to a Fourier series expansion, these higher-order terms also began to carry much more significance when at higher eccentricities. An inability to account for these higher-order terms introduced more and more position error for eccentricities above 0.5, and these unaccounted for frequencies also show up as periodic in all the position residuals. This growth becomes exponential around TC1-9, TC1-10, TC1-11, and TC1-12 (see Figure 4.13, Figure 4.14, Figure 4.15, and Figure 4.16). The fix, obviously, is to include more terms, however, this would require an extensive re-write of the code and how it processes arrays and stores memory. Finally, some of the test cases violated the limits of double precision accuracy (see TC1-1 and TC1-4).

5.2 Conclusions

- The evidence clearly indicates that these particular eccentric orbits do, in fact, lie on KAM tori. Despite the aforementioned limitations, this conclusion is abundantly clear. Residuals between the KAM model and integrated data were consistently below tens of meters up until an eccentricity of 0.5. Furthermore, the evidence seems to suggest that even higher eccentricities lie on KAM tori as well, though this research is unable to demonstrate a statement like this.

- The spectral analysis approach (Laskar's method) outlined in the methodology is sufficient for identifying basis frequencies and, thereby, creating KAM tori. It is the current method of choice, but it may not be the only method for extracting KAM tori. Finding other methods may be a topic for further research.

- Much time, data, and data points are needed for success. Integrating and fitting 4 years of data is non-trivial, and even long times are needed for higher eccentricities. Dedicated computing time and efficient algorithms are essential for reasonable progress.

- Operational satellites may not be able to use KAM theory as a viable method since it requires large chunks of orbital data free of maneuvers. Space debris and "fly and forget" satellites have the opportunity to benefit the most from KAM theory due to long data tracks.

5.3 Final Thoughts and Recommendations

The goal of this research was to answer the following three research questions posed in Chapter 1:

- Can KAM theory be used to model dynamics for earth satellites in highly eccentric orbits?

- Will this method capture a more accurate picture of the true dynamics?

- How accurate are the results?

Bases on the data and results, yes, KAM theory can be used to accurately model dynamics for earth satellites in highly eccentric orbits, and it has been shown to do so up to 0.5 meters of accuracy. This conclusion, of course, only considers the earth's geopotential as the only perturbation. An area of future research is to compare the position vectors of these same orbits with that of actual satellite data, which would have all perturbations inherently included. This would allow one to answer the question, "How much more accurate is the KAM theory method over current methods?" Other topics for future research include a re-write of the code to address the limitations noted in this chapter and an investigation into how resonance features interact with KAM tori.

A method such as KAM tori construction for satellite dynamics could be immediately put into practice for space debris and "fly and forget" satellites if further investigation reveals improvement in accuracy over current methods. Finally, A KAM torus could also be used as the baseline for perturbation theory if not used explicitly. Wiesel has already demonstrated techniques for doing this [24].

5.4   Software and System Specifications

Systems Tool Kit 10.0.2, known mainly by its acronym, STK, was used to set up the test cases for each orbit. STK was particularly useful for generating position and velocity vectors for the integration and KAM torus fits.

The code for the Hamming integrator is called "Split-Integrate-Orbit," aptly named for its backwards and forward integration technique. It is an command line executable, written in C++, designed to output position and velocity vectors into a coordinate file at each time step based on the dynamics of the earth's geopotential. The user has the option to provide a compatible geopotential file as an input to the program; the current research uses EGM96, 20x20.

"Vector-Peak-Eater" is a Laskar algorithm economized for processing vectors from the coordinate file produced by "Split-Integrate-Orbit." It processes each coordinate in

sequence, extracts the highest peaks in sequence, moving towards lower amplitude, and then iterates to remove cross coupling of peaks in clusters on the third frequency. It also outputs KAM torus position data based upon the frequencies it identified. Other information, such as, goodness of fit, Nyquist data, and spectral information are generated by this program. The user has the option to adjust the Fourier series summation limits for each degree of freedom, the Hanning window, and the number of spectral lines. "Vector-Peak-Eater" is also a command line executable written in C++.

"Do-Arb-Residuals" reads the KAM torus file created by "Vector-Peak-Eater" and the data file created by "Split-Integrate-Orbit" and calculates the residuals. It, too, is a command line executable written in C++.

This software was run on a computer with the following system specifications:

- OS/System Type: Windows 7, 64bit

- Processor: Intel(R) Core(TM)i7-2630QM CPU @ 2.00 GHz

- RAM: 8GB

Appendix A: Hamiltonian Error Graphs
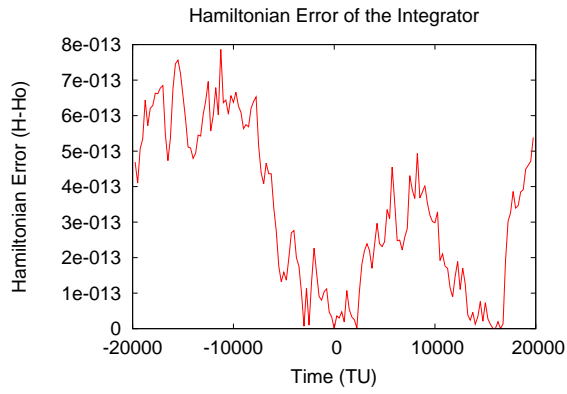
Figure A.1: Hamiltonian Error, TC0-1
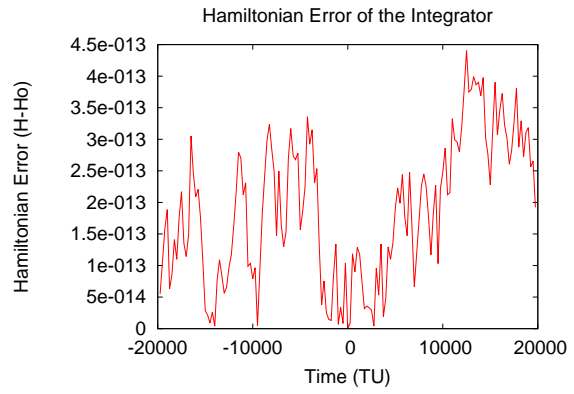
Figure A.2: Hamiltonian Error, TC0-2
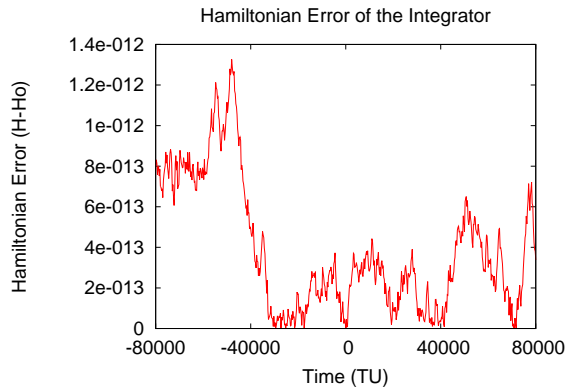
Figure A.3: Hamiltonian Error, TC1-1
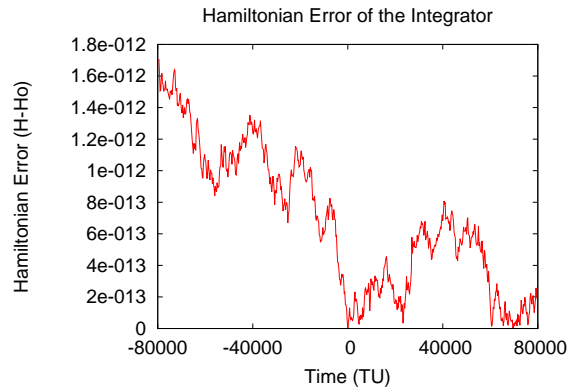
Figure A.4: Hamiltonian Error, TC1-2
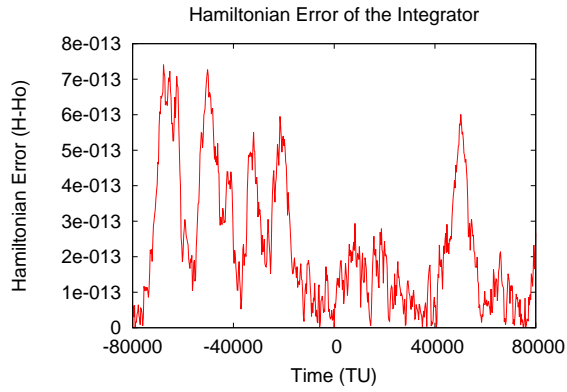
Figure A.5: Hamiltonian Error, TC1-3
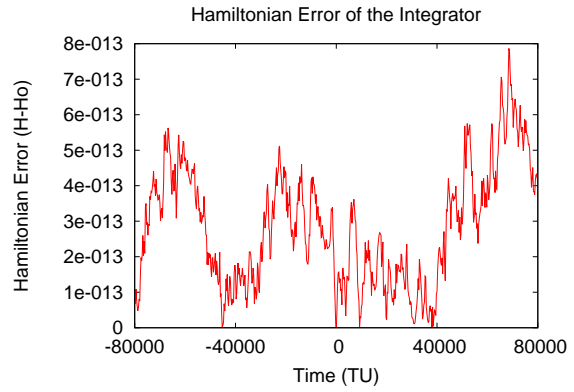
Figure A.6: Hamiltonian Error, TC1-4
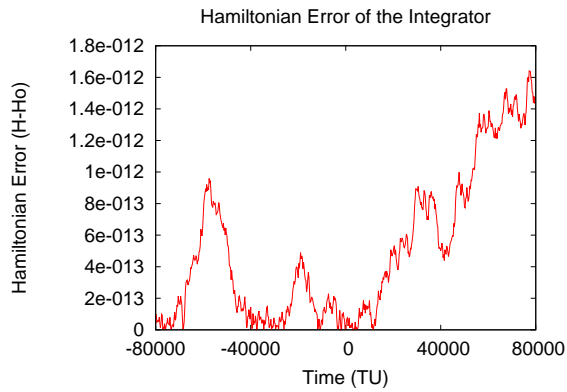
Figure A.7: Hamiltonian Error, TC1-5
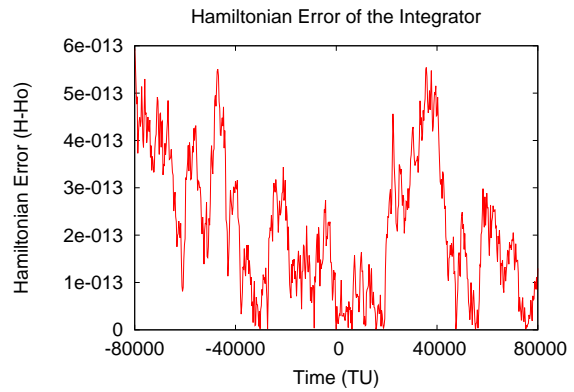
Figure A.8: Hamiltonian Error, TC1-6
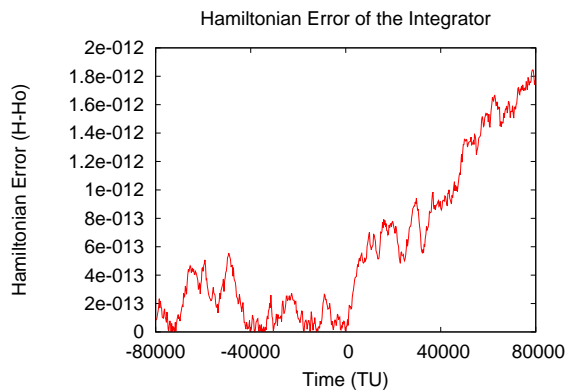
Figure A.9: Hamiltonian Error, TC1-7
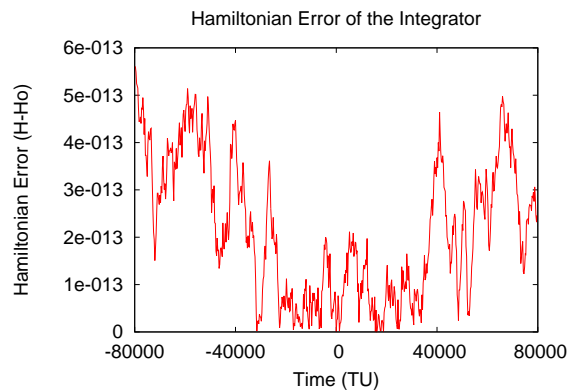
Figure A.10: Hamiltonian Error, TC1-8

69
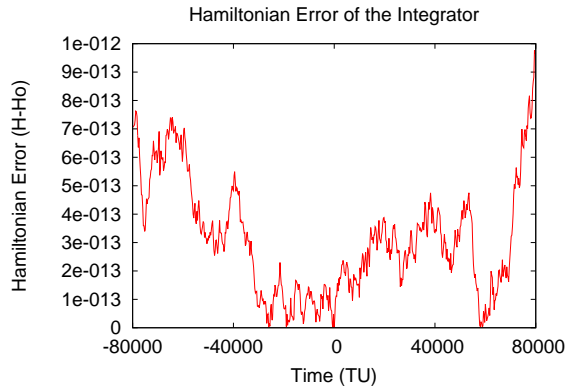
Figure A.11: Hamiltonian Error, TC1-9
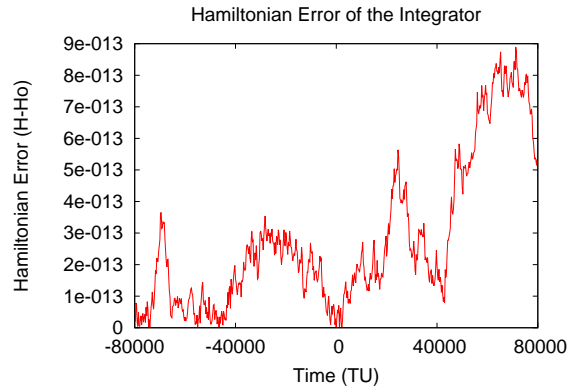
Figure A.12: Hamiltonian Error, TC1-10
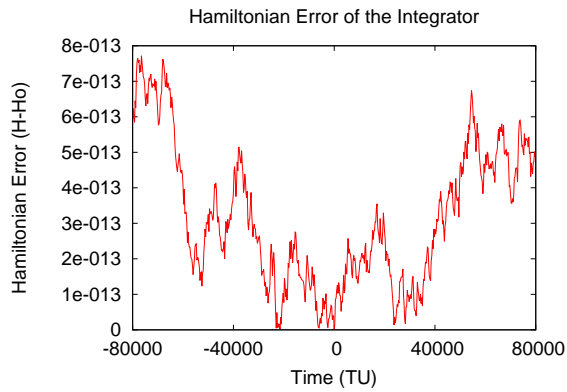
Figure A.13: Hamiltonian Error, TC1-11
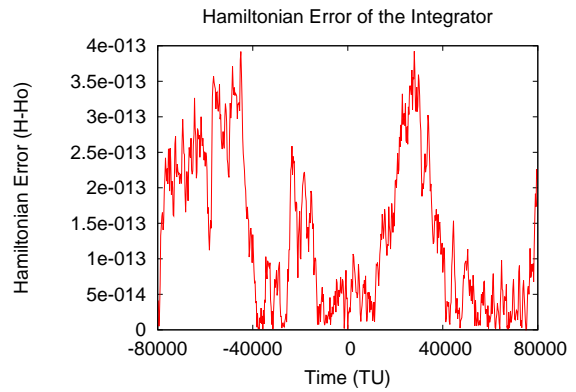
Figure A.14: Hamiltonian Error, TC1-12
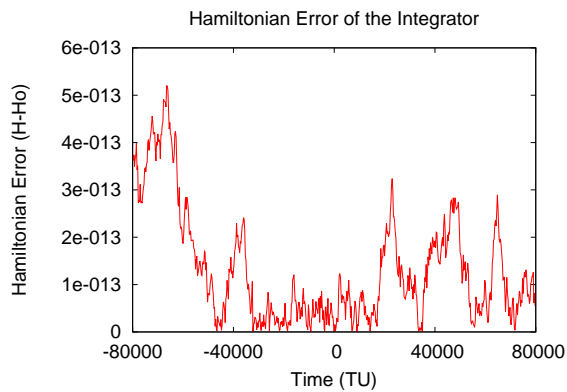
Figure A.15: Hamiltonian Error, TC1-13
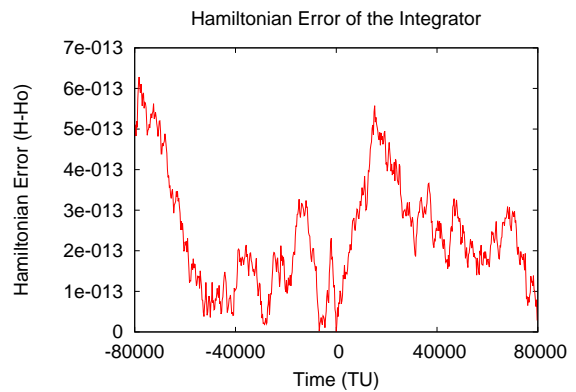
Figure A.16: Hamiltonian Error, TC1-14
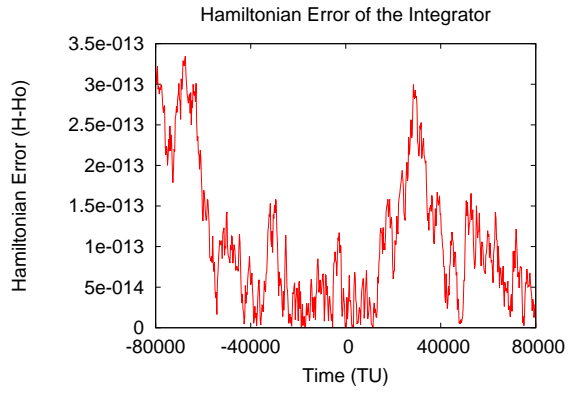
Figure A.17: Hamiltonian Error, TC1-15
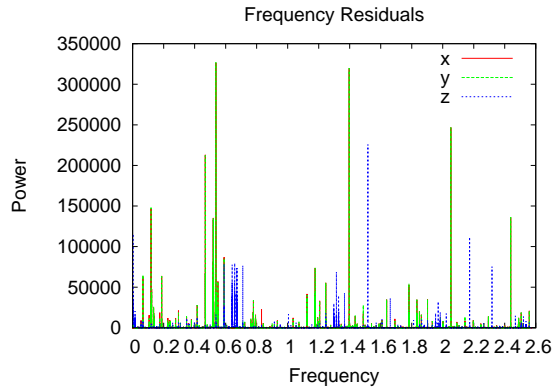
Appendix B: Frequency Residual Graphs
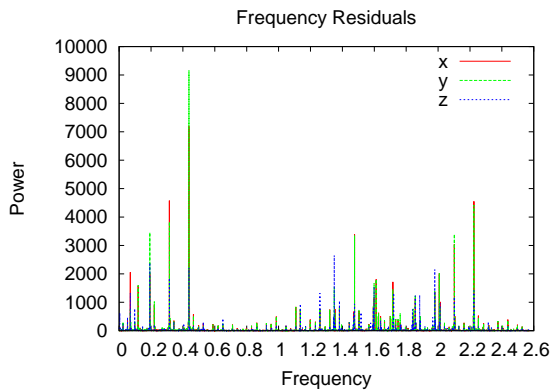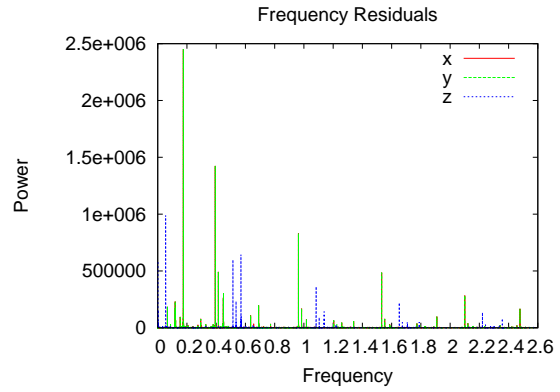

Figure B.1: Frequency Residuals, TC0-1
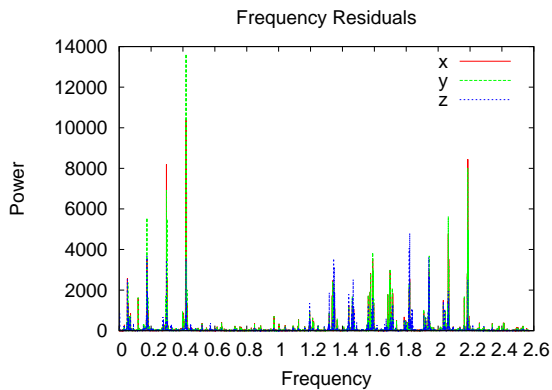
Figure B.2: Frequency Residuals, TC0-2
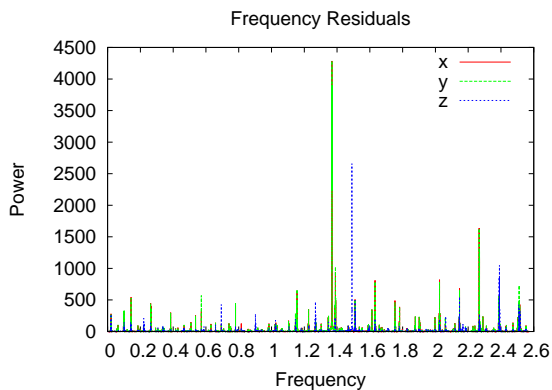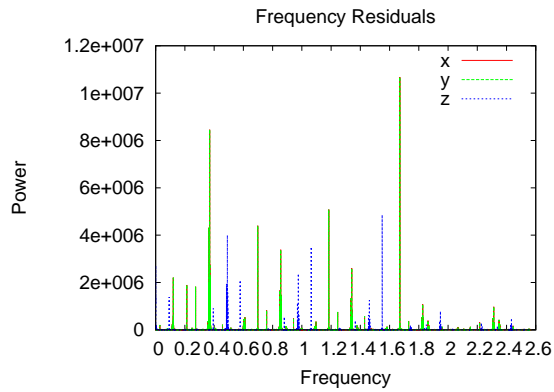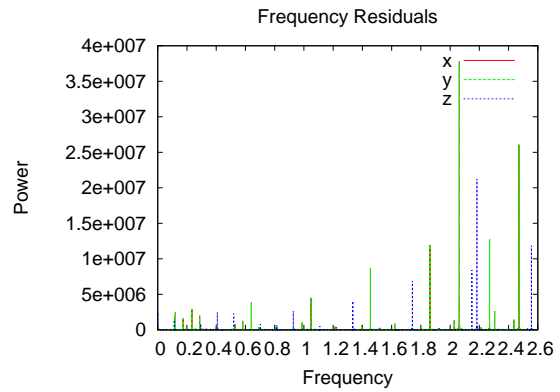

Figure B.3: Frequency Residuals, TC1-1
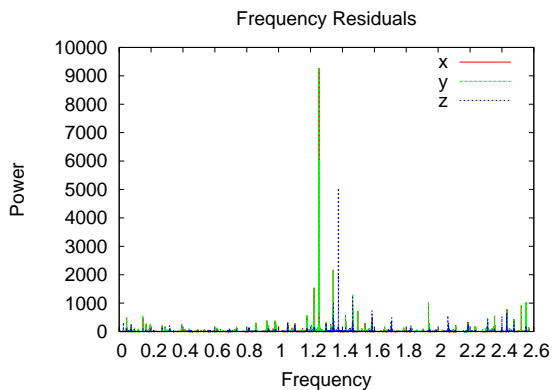
Figure B.4: Frequency Residuals, TC1-2
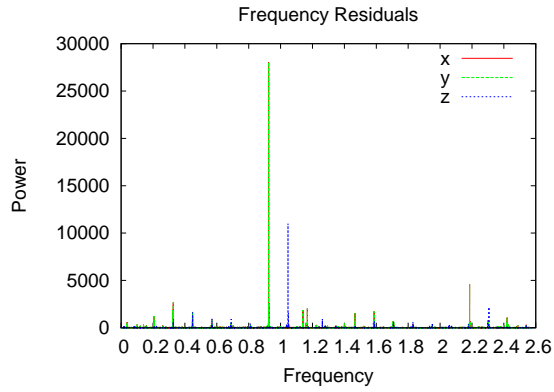
Figure B.5: Frequency Residuals, TC1-3
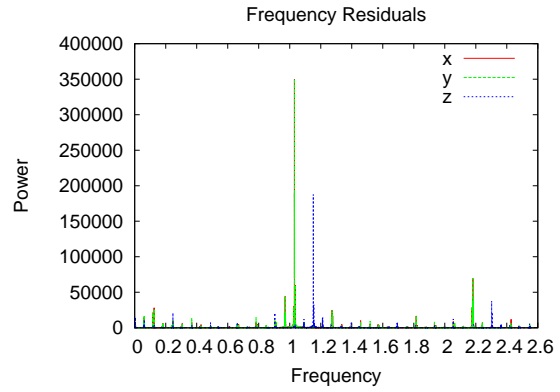
Figure B.6: Frequency Residuals, TC1-4
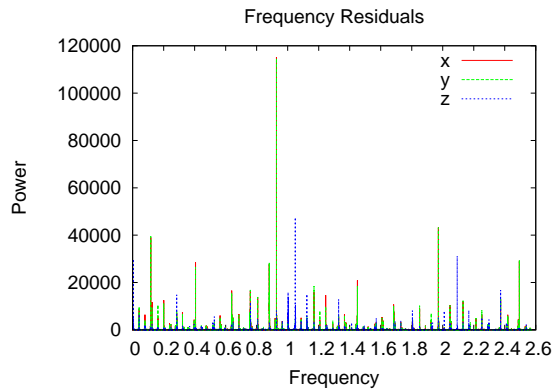
Figure B.7: Frequency Residuals, TC1-5
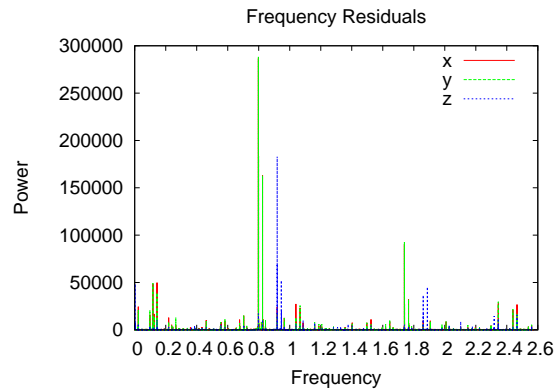
Figure B.8: Frequency Residuals, TC1-6
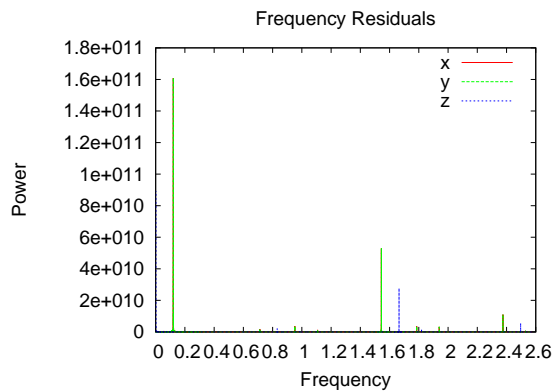
Figure B.9: Frequency Residuals, TC1-7
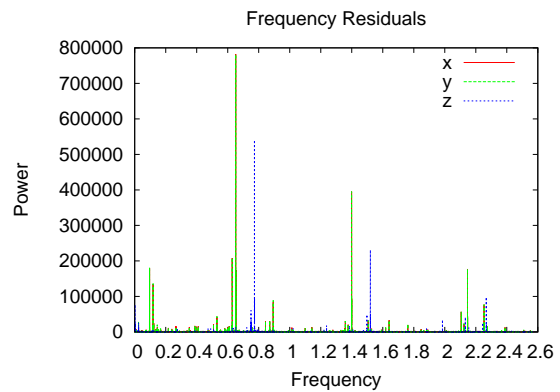
Figure B.10: Frequency Residuals, TC1-8

73

Figure B.11: Frequency Residuals, TC1-9

Figure B.12: Frequency Residuals, TC1-10

Figure B.13: Frequency Residuals, TC1-11
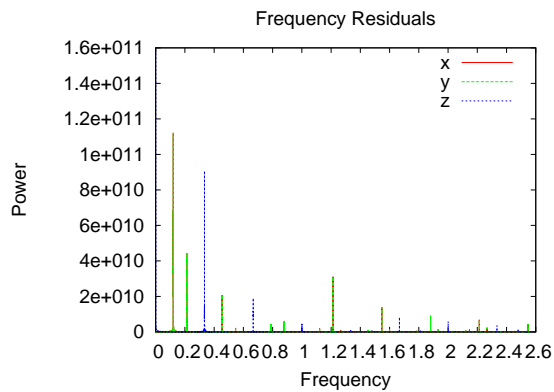

Figure B.14: Frequency Residuals, TC1-12
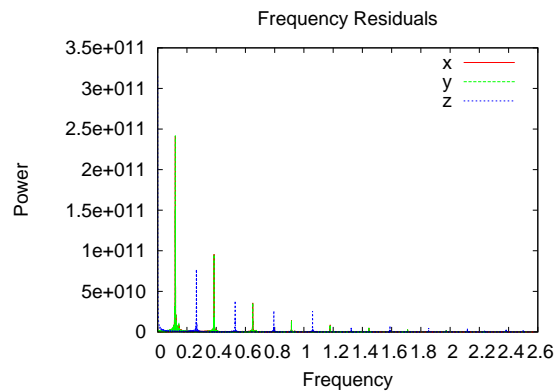

Figure B.15: Frequency Residuals, TC1-13
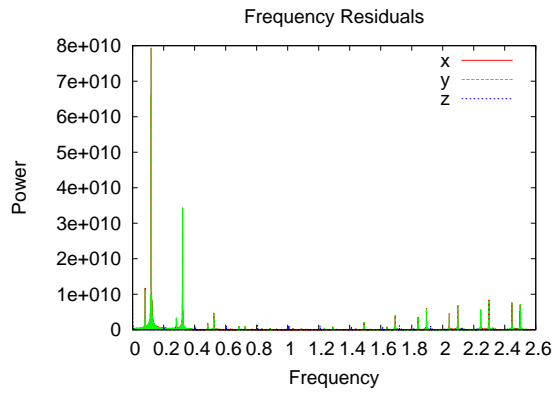

Figure B.16: Frequency Residuals, TC1-14

Figure B.17: Frequency Residuals, TC1-15

Bibliography

[1] "Satellite Collision Leaves Significant Debris Clouds". *NASA Orbital Debris Quarterly News*, 13, April 2009.

[2] Aiton, Eric J. "Kepler's second law of planetary motion". *Isis*, 60(1):75–90, 1969.

[3] Arnol'd, Vladimir Igorevich. "Proof of a Theorem of A. N. Kolmogorov on the Invariance of Quasi- Periodic Motions Under Small Perturbations of the Hamiltonian." *Russ. Math. Surv.*, 18(5):9–36, 1963.

[4] Arnol'd, Vladimir Igorevich. *Mathematical methods of classical mechanics*, volume 60. Springer, 1989.

[5] Bordner, Ralph E. *Orbital Tori Construction Using Trajectory Following Spectral Methods*. Ph.D. thesis, Air Force Institute of Technology, September 2010.

[6] Celletti, Alessandra and Luigi Chierchia. "KAM Stability Estimates in Celestial Mechanics". *Planet. Space Sci.*, 46:1433–1440, 1998.

[7] Celletti, Alessandra and Luigi Chierchia. "KAM Tori for N-body Problems: A Brief History". *Celestial Mechanics and Dynamical Astronomy*, 95:117–139, 2006.

[8] Craft, Christopher T. *Formation Flight of Earth Satellites on KAM Tori*. Master's thesis, Air Force Institute of Technology, September 2009.

[9] Ely, Todd A and Kathleen C Howell. "East-west stationkeeping of satellite orbits with resonant tesseral harmonics". *Acta Astronautica*, 46(1):1–15, 2000.

[10] Féjoz, Jacques. "Dèmonstration du 'théorème d'Arnol'd' sur la stabilité du système planétaire (d'après Herman)". *Ergodic Theory Dynam. Systems*, 5:1521–1582, 2004.

[11] Gidea, Marian, James Meiss, Ilie Ugarcovici, and Howard Weiss. "Applications of KAM theory to Population Dynamics". *Journal of Biological Dynamics*, 5:44–63, 2011.

[12] Hunter, C. "Spectral analysis of orbits via discrete Fourier transforms". *Space science reviews*, 102(1-4):83–99, 2002.

[13] Kolmogorov, Andrey. N. "The Conservation of Conditionally Periodic Motions with a Small Variation in the Hamiltonian". *Doklady Akademii nauk SSSR*, 98:527–530, 1954.

[14] Laskar, Jacques. "Introduction to frequency map analysis". *Hamiltonian systems with three or more degrees of freedom*, 134–150. Springer, 1999.

[15] Laskar, Jacques. "Frequency Map Analysis and Quasiperiodic Decompositions". *Proceedings of Proquerolles School*, 1–31, 2001.

[16] Little, Brian. *Application of KAM Theorem to Earth Orbiting Satellites*. Master's thesis, Air Force Institute of Technology, September 2009.

[17] Meirovitch, Leonard. *Methods of analytical dynamics*. DoverPublications, 2010.

[18] Moser, Juergen. "On Invariant Curves of Area Preserving Mappings of an Annulus". *Nachrichten der Akademie der Wissenschaften in Gottingen. II*, K1. II.:1–20, 1962.

[19] Vallado, David A. *Fundamentals of Astrodynamics and Applications*. Microcosm Press and Kluwer Academic Publishers, second edition, 2001.

[20] Wiesel, William E. *Modern Astrodynamics*. Aphelion Press, 2003.

[21] Wiesel, William E. "Earth Satellite Orbits As KAM Tori". *The Journal of the Astronautical Sciences*, 56(2):151–162, 2008.

[22] Wiesel, William E. *KAM Tori Construction Algorithms*. Technical report, DTIC Document, August 2008.

[23] Wiesel, William E. *KAM Tori Normal Coordinates*. Technical report, DTIC Document, January 2009.

[24] Wiesel, William E. *Earth Satellite Perturbation Theories as Approximate KAM Tori*. Technical report, DTIC Document, January 2010.

REPORT DOCUMENTATION PAGE

1. REPORT DATE *(DD–MM–YYYY)*	2. REPORT TYPE		3. DATES COVERED *(From — To)*
27–03–2014	Master's Thesis		Oct 2012–Mar 2014

4. TITLE AND SUBTITLE	5a. CONTRACT NUMBER
Applying KAM Theory to Highly Eccentric Orbits	5b. GRANT NUMBER
	5c. PROGRAM ELEMENT NUMBER

6. AUTHOR(S)	5d. PROJECT NUMBER
Dunk, Adam B., Captain, USAF	5e. TASK NUMBER
	5f. WORK UNIT NUMBER

7. PERFORMING ORGANIZATION NAME(S) AND ADDRESS(ES)	8. PERFORMING ORGANIZATION REPORT NUMBER
Air Force Institute of Technology	
Graduate School of Engineering and Management (AFIT/EN)	
2950 Hobson Way	AFIT-ENY-14-M-19
WPAFB, OH 45433-7765	

9. SPONSORING / MONITORING AGENCY NAME(S) AND ADDRESS(ES)	10. SPONSOR/MONITOR'S ACRONYM(S)
	11. SPONSOR/MONITOR'S REPORT NUMBER(S)

12. DISTRIBUTION / AVAILABILITY STATEMENT

DISTRIBUTION STATEMENT A:
APPROVED FOR PUBLIC RELEASE; DISTRIBUTION UNLIMITED

13. SUPPLEMENTARY NOTES

14. ABSTRACT

THIS research applies KAM theory to highly eccentric orbits for earth orbiting satellites by using spectral methods to find the three basis frequencies resulting from earth's geopotential. Once a torus is created from these frequencies, its dynamics data can be compared to the position data of an integrated data set over multiple orbit types, specifically, orbits with varying eccentricity. The analysis shows that many eccentric orbits are actually KAM tori when the only perturbation is the earth's geopotential. The residuals agree to 10s of meters in most cases. This research also outlines many of the limitations of the current method and gives recommendations for further study and real-world applications. Applications focus on space debris and non-operational satellites.

15. SUBJECT TERMS

KAM Theory, Tori, Orbits, Spectral Methods

16. SECURITY CLASSIFICATION OF:			17. LIMITATION OF ABSTRACT	18. NUMBER OF PAGES	19a. NAME OF RESPONSIBLE PERSON
a. REPORT	b. ABSTRACT	c. THIS PAGE			Dr. William E. Wiesel Jr. (ENY)
U	U	U	UU	94	19b. TELEPHONE NUMBER *(include area code)* (937) 255-3636 x4312 william.wiesel@afit.edu